

Homogeneous abundance analysis of dwarf, subgiant and giant FGK stars with and without giant planets ^{★, ★★}

Ronaldo da Silva^{1,2}, André de C. Milone¹, and Helio J. Rocha-Pinto³

¹ Divisão de Astrofísica, Instituto Nacional de Pesquisas Espaciais, São José dos Campos, Brazil

² Dipartimento di Fisica, Università di Roma Tor Vergata, Rome, Italy

³ Observatório do Valongo, Universidade Federal do Rio de Janeiro, Rio de Janeiro, Brazil

Received / accepted

ABSTRACT

Aims. We have analyzed high-resolution and high signal-to-noise ratio optical spectra of nearby FGK stars with and without detected giant planets in order to homogeneously measure their photospheric parameters, mass, age, and the abundances of volatile (C, N, and O) and refractory (Na, Mg, Si, Ca, Ti, V, Mn, Fe, Ni, Cu, and Ba) elements. Our sample contains 309 stars from the solar neighborhood (up to the distance of 100 pc), out of which 140 are dwarfs, 29 are subgiants, and 140 are giants.

Methods. The photospheric parameters are derived from the equivalent widths of Fe I and Fe II lines. Masses and ages come from the interpolation in evolutionary tracks and isochrones on the HR diagram. The abundance determination is based on the equivalent widths of selected atomic lines of the refractory elements and on the spectral synthesis of C₂, CN, C I, O I, and Na I features. We apply a set of statistical methods to analyze the abundances derived for the three subsamples.

Results. Our results show that: *i*) giant stars systematically exhibit underabundance in [C/Fe] and overabundance in [N/Fe] and [Na/Fe] in comparison with dwarfs, a result that is normally attributed to evolution-induced mixing processes in the envelope of evolved stars; *ii*) for solar analogs only, the abundance trends with the condensation temperature of the elements are correlated with age and anticorrelated with the surface gravity, which is in agreement with recent studies; *iii*) as in the case of [Fe/H], dwarf stars with giant planets are systematically enriched in [X/H] for all the analyzed elements, except for O and Ba (the former due to limitations of statistics), confirming previous findings in the literature that not only iron has an important relation with the planetary formation; and *iv*) giant planet hosts are also significantly overabundant for the same metallicity when the elements from Mg to Cu are combined together.

Key words. stars: fundamental parameters - stars: abundances - planetary systems - methods: data analysis - techniques: spectroscopic

1. Introduction

The fact that stars hosting a giant planet are, on average, more abundant in iron than stars in the solar neighborhood for which no planet has been detected (Santos et al. 2001, 2004; Fischer & Valenti 2005; Gonzalez 2006) is well accepted. Actually, it has been shown that this behavior is not exclusive to iron but it is shared by several other metals (Bond et al. 2006; Gilli et al. 2006; Neves et al. 2009; Adibekyan et al. 2012b). Other studies also suggested that this kind of anomaly may not only involve the metal content of heavy elements but also some light elements such as carbon, nitrogen, and oxygen (Ecuavillon et al. 2004, 2006; Petigura & Marcy 2011).

Some authors have also been searching for differences in the abundance trends with metallicity for several elements in stars with and without planets. In other words, these works investigated whether the planetary formation in some way affects the observed abundances by comparing stars in the same metallicity range. Robinson et al. (2006) reported that the [Si/Fe] and [Ni/Fe] abundance ratios in planet-host stars are systematically

enhanced over their comparison sample of stars without planets of the same metallicity. Delgado Mena et al. (2010) derived the opposite behavior for Mg, and they found no differences regarding [C/Fe], [O/Fe] and [Si/Fe]. In any case, they stated that their result for Mg disappears when only solar analogs are considered. Neves et al. (2009) also reported no significant differences in [X/Fe] for 12 elements in stars with and without planets. Gonzalez & Laws (2007) derived lower [Al/Fe] and [Si/Fe] but higher [Ti/Fe] in stars with planets in the range of metal-rich stars. Brugamyer et al. (2011), on the other hand, confirmed the [Si/Fe] enhancements in planet hosts, in spite of no [O/Fe] enhancements. Overabundances of several elements were also reported by Kang et al. (2011) and Adibekyan et al. (2012a), but only in the range of metal-poor stars, except for Mn. For this element, Kang et al. (2011) found an enhancement in the whole range of metallicity, a result that is not supported by Adibekyan et al. (2012a). The situation is, therefore, vast and varied, and also controversial for some elements.

In a previous paper (da Silva et al. 2011, from now on referred to as Paper 1) we determined photospheric parameters and carbon abundances for a sample of 172 dwarf, subgiant, and giant stars (out of which 18 with planets) using spectra available in the ELODIE database (Moultaka et al. 2004). Our previous results did not point out, for instance, any significant difference between the carbon abundances of stars with and without planets, for the three substellar groups. However, the analyzed sam-

Send offprint requests to: R. da Silva,
e-mail: ronaldo.dasilva@roma2.infn.it

* Based on public data from the ELODIE archive (Moultaka et al. 2004, online access: <http://atlas.obs-hp.fr/elodie/>)

** Tables 4-8 are only available in electronic form at the CDS via anonymous ftp to cdsarc.u-strasbg.fr (130.79.128.5) or via <http://cdsweb.u-strasbg.fr/cgi-bin/qcat?J/A+A/>

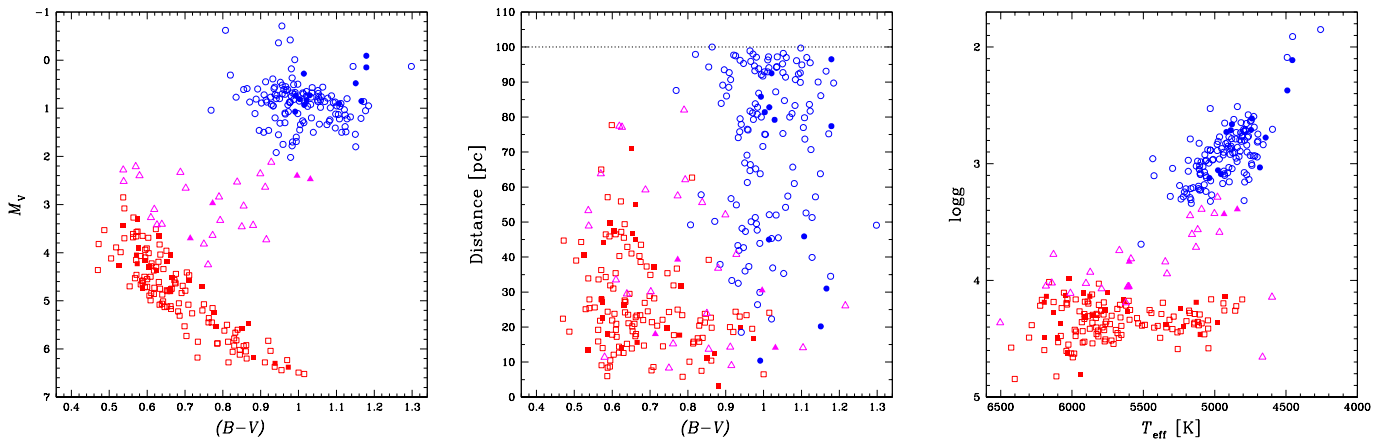


Fig. 1. HR (left panel) and color-distance (middle panel) diagrams for our sample of 140 dwarfs (\square), 29 subgiants (\triangle), and 140 giants (\circ). The derived stellar parameters are also shown in a $\log g$ vs. T_{eff} diagram (right panel) for comparison. Filled symbols represent stars with detected planets. The distance limit of 100 pc is represented by the dotted line.

ple was quite small to provide conclusive results, and stimulated the inclusion of additional stars and other chemical elements.

In the current work we have 309 FGK stars (out of which 47 with detected planets) homogeneously analyzed in order to measure their photospheric parameters, masses, ages, and the abundances of volatile (C, N, and O) and refractory (Na, Mg, Si, Ca, Ti, V, Mn, Fe, Ni, Cu, and Ba) elements. The sample includes dwarf, subgiant, and giant stars, mostly belonging to the Galactic thin disc. We have applied a set of statistical methods to the three subsamples, exploring their multivariate properties and, in particular, uncovering significant differences between dwarf stars with and without a known giant planet. In addition, we have searched for relations involving the stellar parameters, the abundances, and the condensation temperature of the elements. This approach has been very often used in order to check whether any difference in the amount of refractory elements with respect to volatile ones has an influence on the formation of planetary systems (see, e.g., Smith et al. 2001; Meléndez et al. 2009; Ramírez et al. 2009; González Hernández et al. 2010, 2013a,b).

In Sect. 2 we describe the observations and the procedure of data reduction. In Sect. 3 we outline the methods used to derive the photospheric parameters and the chemical abundances. The determination of the evolutionary and the kinematic parameters is presented in Sect. 4. The results are presented and discussed in Sect. 5 and in Sect. 6, in which we describe the statistical analysis. Finally, we present our final remarks and conclusions in Sect. 7.

2. Observation data and reduction

In this work, as a complement to our previous analysis of 172 stars published in Paper 1, we have enlarged our stellar sample. Now we have 309 FGK stars from the solar neighborhood that include 140 dwarfs (out of which 31 with detected planets), 29 subgiants (4 with planets), and 140 giants (12 with planets).

The stars were observed with the ELODIE high-resolution spectrograph (Baranne et al. 1996) of the Haute Provence Observatory (France), and the data are publicly available in the online ELODIE database. The ELODIE spectrograph provides spectra with resolution $R \sim 42\,000$ in the wavelength range 3895–6815 Å. The criteria of selection are similar, but not equal, to those applied before since we have now considered a smaller

inferior limit for the signal-to-noise ratio (S/N). Following this new criteria we selected:

- i) stars for which the averaged spectra have $S/N \geq 150$; only individual spectra with a $S/N \geq 20$ and with an image type classified as *object fibre only* (OBJO) were used;
- ii) stars within a distance ≤ 100 pc (parallax $\pi \geq 10$ mas) and with spectral type between F8 and M1;
- iii) stars having no close-in binary companion that could contaminate the observed spectra; we used the information of the angular separation between components (ρ) available in the Hipparcos catalogue (ESA 1997) and we chose only the systems with $\rho > 10$ arcsec; additionally, we searched in literature for any further information that could unveil a contaminant star in the observed field;
- iv) stars with $(B - V)$ measured by Hipparcos and with cross-correlation parameters available in the ELODIE database; both $(B - V)$ and the width of the spectral cross-correlation function are required to carry out a first estimate of the projected rotation velocity $v \sin i$ of each star; and
- v) stars for which the determination of the photospheric parameters is reliable (see Sect. 3.1) and that passed the quality control of the spectral synthesis (see Sect. 3.2).

A total of 1485 spectra of 309 stars has been analyzed. The subsamples of dwarfs, subgiants, and giants are plotted in the HR and color-distance diagrams of Fig. 1. As in Paper 1, we chose to classify as subgiants those stars situated 1.5 mag above the lower limit of the main-sequence and having $M_v > 2.0$ mag. Note that the distance of dwarfs and subgiants is not limited to 100 pc, but to about 80 pc, which represents a selection effect of the ELODIE observation surveys. For comparison, in the right panel of this figure we plot the $\log g$ vs. T_{eff} diagram with the stellar parameters derived in the current work.

The spectra were reduced using IRAF¹ routines for order identification and extraction, background subtraction, flat-field correction, wavelength calibration, radial-velocity shift correction, and flux normalization (a global normalization first, and then a more careful one performed around regions containing molecular bands and atomic lines used in the spectral synthesis).

¹ *Image Reduction and Analysis Facility*, distributed by the National Optical Astronomy Observatories (NOAO), USA.

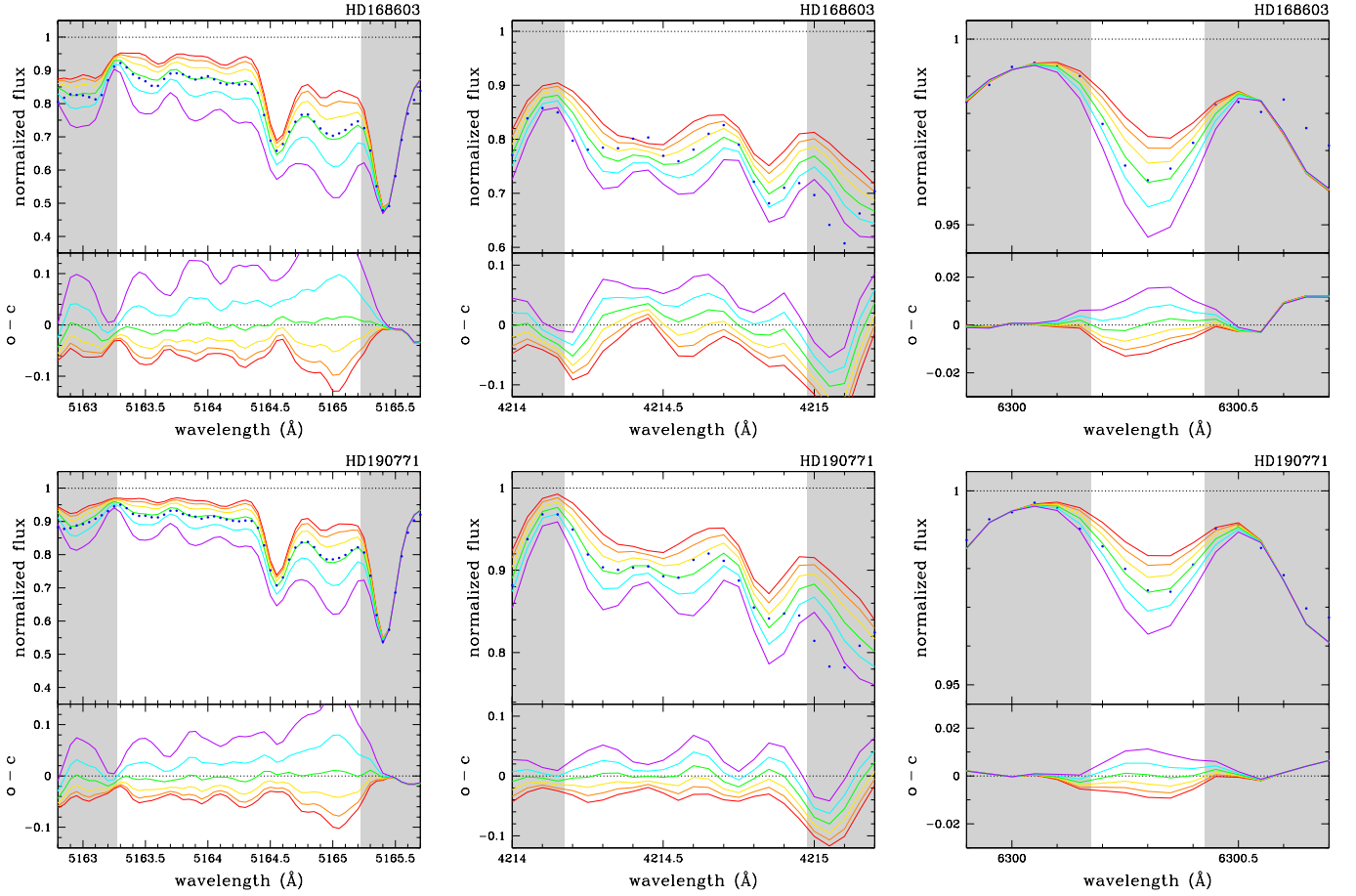


Fig. 2. Synthesis of three spectral regions: C_2 ($\lambda 5165$, left panels) and CN ($\lambda 4215$, middle panels) molecular band heads, and the O atomic line at $\lambda 6300.30$ (right panels). Two dwarf stars with different values of spectral S/N are shown: HD 168603 (S/N = 156, $T_{\text{eff}} = 5399$ K, $[Fe/H] = 0.11$ dex, top panels) and HD 190771 (S/N = 299, $T_{\text{eff}} = 5817$ K, $[Fe/H] = 0.14$ dex, bottom panels). These are the S/N per pixel computed at $\lambda 5550$. Six spectra computed for different abundances (the N abundance is changed in the case of the CN band) and separated by 0.1 dex are plotted. The differences between observed and computed spectra (O–C) are also plotted in the bottom of each panel.

3. Spectroscopic analysis

3.1. Photospheric parameters and equivalent widths

In this work, as in Paper 1, we performed a differential analysis relative to the Sun. The method requires a model atmosphere for each star, which in turn is computed using the so-called photospheric parameters: effective temperature T_{eff} , metallicity $[Fe/H]$, surface gravity $\log g$, and microturbulent velocity ξ . We computed these parameters through the excitation equilibrium of neutral iron and the ionization equilibrium between Fe I and Fe II lines, using model atmospheres derived by interpolation in the grid of Kurucz (1993). As before, we used the MOOG LTE radiative code (Snedden 2002) and the same routine developed by us to perform an automated calculation of the parameters and their uncertainties, allowing a fast and homogeneous approach.

To compute the solar model atmosphere we adopted $T_{\text{eff}} = 5777$ K, $\log g = 4.44$, $\xi = 1.0$ km s $^{-1}$, and the standard solar abundances of Anders & Grevesse (1989), but with $\log \epsilon_{\odot}(Fe) = 7.47$ to be consistent with the value adopted in Paper 1. We also assumed the Unsöld approximation multiplied by 6.3 to account for the van der Waals line damping. This is useful for a better treatment of strong lines close to the spectral windows used in our spectral synthesis analysis.

The atomic line parameters (wavelength, statistical weight of the lower level multiplied by the oscillator strength gf , and lower-level excitation potential χ) of 71 Fe I and 12 Fe II lines are listed in Table 2. The table also lists the parameters of the other elements analyzed by means of their equivalent width (EW). Table 3 contains the gf values of the elements with important hyperfine structure (HFS). These parameters were initially taken from the *Vienna Atomic Line Database – VALD* (Kupka et al. 2000, 1999; Piskunov et al. 1995; Ryabchikova et al. 1997) in the case of the elements without HFS, and from Steffen (1985) for those with important HFS. The gf values were then revised in order to fit the equivalent widths measured in the spectrum of the Solar Flux Atlas (Kurucz et al. 1984) degraded to the ELODIE resolution. For the Sun and for all the other stars of our sample, the EW s were measured using the *Automatic Routine for line Equivalent widths in stellar Spectra – ARES* (Sousa et al. 2007), and they are also listed in Table 2.

The atomic lines of the elements Mg, V, Mn, and Cu have important HFS that has to be taken into account. In the case of those elements with lines not listed in Steffen (1985), we adopted the values of neighboring multiplets. An exception is the Mg line at $\lambda 5785.29$, for which no HFS information was available. Its gf value was obtained in the same way as those lines without HFS listed in Table 2. This line is not strong ($EW < 60$ mÅ) and the

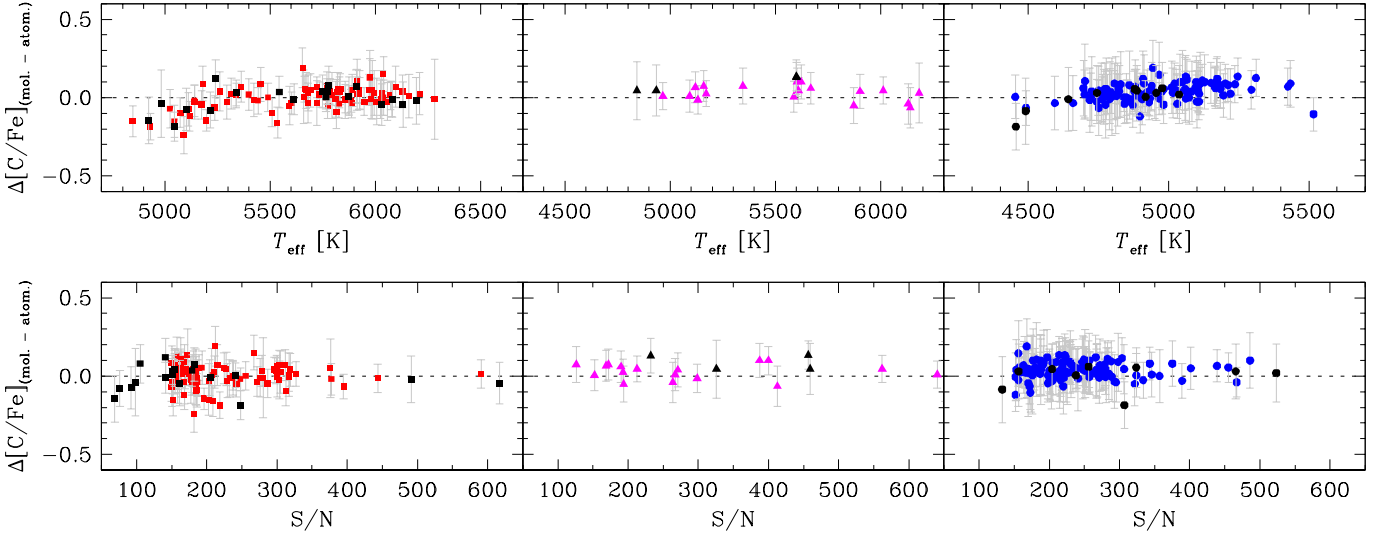


Fig. 3. Difference between the C abundances derived from the C₂ molecular bands (λ 5128 and λ 5165) and the C atomic line (λ 5380.34) as a function of the effective temperature (top panels) and of the S/N (bottom panels) for our sample of dwarfs (left panels), subgiants (middle panels), and giants (right panels). Stars with planets are represented by black symbols.

error induced in the Mg abundance determination is of second order. The HFS of Ba, and also its isotopic splitting, are of some importance but only for the line at λ 6496.91, being negligible for the lines at λ 5853.69 and λ 6141.73 (see Korotin et al. 2011).

Table 4 shows an excerpt of the derive photospheric parameters for the 140 dwarf stars in our sample, together with their uncertainties. The complete tables, also for subdwarfs and giants, are available in electronic form at the CDS.

3.2. Abundance determination

The abundances of the refractory elements (Na, Mg, Si, Ca, Ti, V, Mn, Ni, Cu, and Ba), with respect to Fe, were determined based on the equivalent widths of a selection of spectral lines chosen as being free from blends by inspection of the Solar Flux Atlas and the solar line identifications catalogue of Moore et al. (1966).

We used the *abfind* (in the case of elements without important HFS), and the *blends* (in the case of elements with HFS) drivers of the MOOG code to derive the abundances. These drivers require: (i) the model atmospheres, which were previously computed using the photospheric parameters derived for each star; and (ii) a list of the selected lines, containing the respective wavelength (or the hyperfine structure), the atomic number, the lower-level excitation potential, the revised values of *gf*, and the measured equivalent widths. Again, using another routine for an automated calculation developed by us, we derived the abundances for each element in turn, excluding when needed (by means of a sigma-clipping procedure) spectral lines that provided a bad abundance determination.

For the volatile elements (C, N, and O), and for Na as well, we used the spectral synthesis technique, also performed with the MOOG code, to reproduce the observed spectra in regions containing molecular lines of electronic-vibrational band heads of the C₂ Swan system (centered at λ 5128 and λ 5165), of the CN blue system (centered at λ 4215), and to atomic lines of C (λ 5380.34), O (λ 6300.30), and Na (λ 6154.23 and λ 6160.75). Again, as in Paper 1, we preferred not to use the C atomic line at

λ 5052.17 because it is blended with a strong Fe line, which may affect the abundance determination.

The synthetic spectra were computed in wavelength steps of 0.01 Å, also considering the continuum opacity contribution in ranges of 0.5 Å, line-broadening corrections (from velocity fields and instrumental broadening), and the limb darkening effect. Some parameters of atomic and molecular spectral lines were taken from the VALD database and from Kurucz (1995), respectively. Additional molecules that contribute to the spectral line formation in the studied wavelength regions are MgH (at λ 5128, λ 5165, and for the C atomic line), CH (at λ 4215), and CN (for the Na and O atomic lines), though their contributions are relatively small. The *gf* values of some atomic and molecular lines were revised to fit the solar spectrum, which was taken as a reference in our differential chemical analysis. The oxygen line at λ 6300.30 is blended with a Ni line at λ 6300.34 ($\log gf = -2.3098$). Therefore, we derived the O abundances by taking the Ni abundance of each star into account when fitting the observed profile. Moreover, to account for the presence of telluric lines in this region, we adopted the telluric spectrum by Wallace et al. (2011), with the resolution degraded to match our spectra.

To account for spectral line broadening from velocity fields, as in Paper 1, we adopted the same definition of V_{broad} (also listed in Table 4), which is a composite of velocity fields, such as rotation and macro-turbulent velocities. The instrumental broadening was estimated from the width of thorium lines, and the linear coefficient *u* of the stellar limb darkening was taken from Díaz-Cordovés (1995).

Figure 2 shows the spectral synthesis applied to three of the regions used for abundance determination, the C₂ (λ 5165) and CN (λ 4215) molecular band heads and the O atomic line at λ 6300.30, for two dwarf stars with different spectral S/N. The synthetic spectra were resampled in steps of 0.05 Å to consistently match the wavelength scale of the observed spectra. For examples of spectral synthesis applied to other regions and to other stars, we refer the reader to Fig. 3 and 5 of Paper 1.

For a comparison between the results provided by molecular- and atomic-line C abundances, Fig. 3 shows the differences plotted as a function of T_{eff} and of S/N for our subsamples of dwarfs,

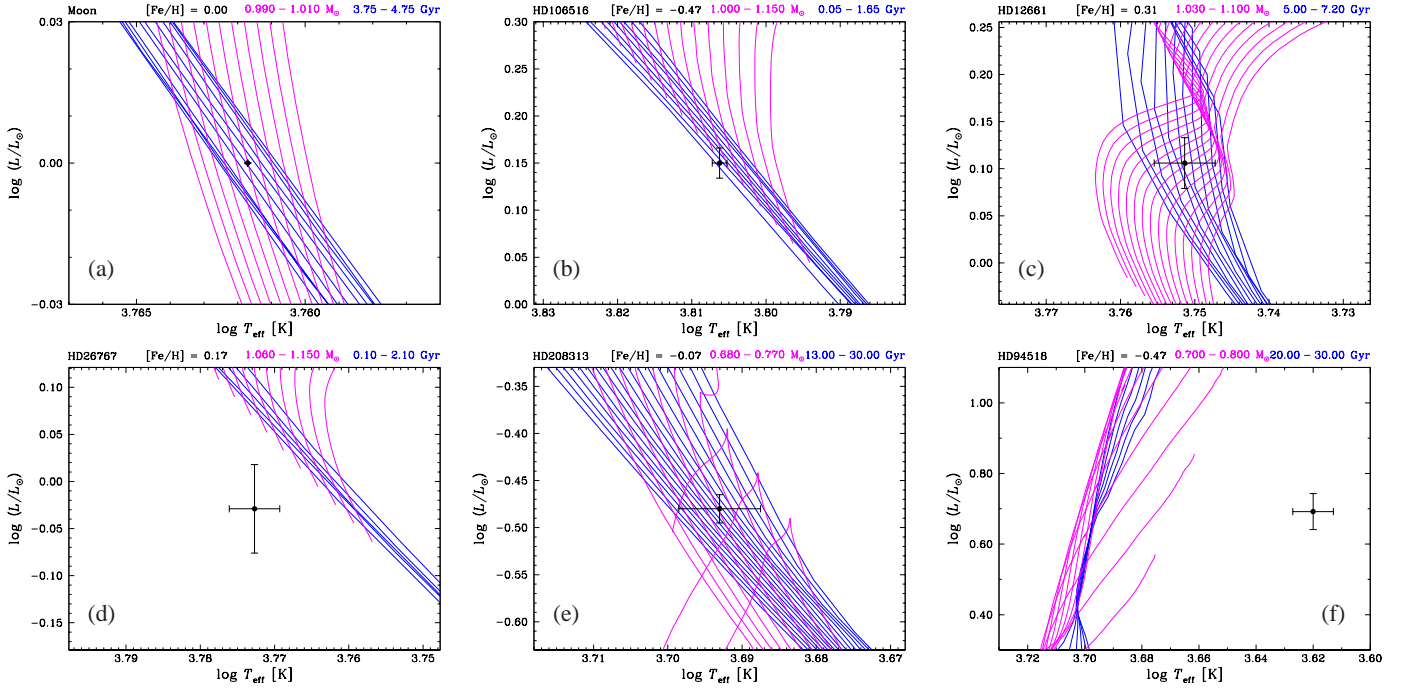


Fig. 4. Evolutionary tracks (magenta lines) and isochrones (blue lines) from Yonsei-Yale, calculated for different values of metallicity, showing how we derived the stellar masses and ages. The ranges of age (increasing from left to right, HD 94518 excepted) and mass (increasing from right to left, HD 94518 excepted) of the models plotted are indicated on the top of each panel.

subgiants, and giants. Besides a slight underabundance (within errors, however) of molecular with respect to atomic C abundances for cool dwarfs, no systematic difference is observed in the whole range of T_{eff} or S/N.

We estimated the uncertainties in the same way as in Paper 1, i.e., using our routine that includes the error propagation of the input parameters used by MOOG: the photospheric parameters T_{eff} , $\log g$, $[\text{Fe}/\text{H}]$, and ξ , and the broadening velocity V_{broad} . Each one in turn, the input parameters are iteratively changed by their errors, and new values of abundance are computed. The difference between new and best determination gives the error due to each parameter uncertainty, and $\sigma([\text{X}/\text{Fe}])$ is a quadratic sum of individual contributions. The error in V_{broad} was estimated to be of the order of 1 km s^{-1} or smaller.

Table 4 shows an excerpt with the derived $[\text{Ti}/\text{Fe}]$ abundance ratios for the 140 dwarf stars. The complete tables with abundances of all the other elements, also for subdwarfs and giants, are available in electronic form at the CDS. The parameters of atomic and molecular lines are listed in Tables 5 and 6, which are only available in electronic form at the CDS as well. Table 5 contains the wavelength of the spectral feature, the atomic and molecular line identification, the lower-level excitation potential, the gf values, and the dissociation energy D_0 (for molecular features only). Table 6 (strong atomic lines) contains the same information of Table 5, except the dissociation energy parameter.

4. Evolutionary and kinematic parameters

4.1. Stellar masses and ages

We derived masses and ages through interpolations in the grids of Yonsei-Yale (Y^2) evolutionary tracks and isochrones (Yi et al. 2001; Kim et al. 2002) on the HR diagram. The determination of these parameters takes into account the metallicity of each star. The stars' luminosities used in the diagrams were calculated

with parallaxes taken from the new reduction of the Hipparcos data (van Leeuwen 2007), and bolometric corrections (BC) from Flower (1996), which were revised by Torres (2010). For the Sun, we adopt $BC_{\odot} = -0.07$ and $M_{\text{bol}}^{\odot} = 4.75$.

A few examples for different metallicities are illustrated in Fig. 4. To reproduce the Sun's position in the HR diagrams, adopting $T_{\text{eff}} = 5777 \text{ K}$ and age = 4.53 Gy (Guenther & Demarque 1997), the evolutionary tracks and isochrones were displaced in $\log(T_{\text{eff}})$ by 0.001628 ($\sim 22 \text{ K}$ in T_{eff}) and in $\log(L/L_{\odot})$ by 0.011. By doing so, we derived for the Sun a mass $M = 1.003 \pm 0.004 M_{\odot}$, and an age = $4.37 \pm 0.17 \text{ Gyr}$ (see Fig. 4a). The figure also shows: a metal-poor and young star (HD 106516, Fig. 4b); a metal-rich one (HD 12661, Fig. 4c); a young star that is outside the lower border of the models (HD 26767, Fig. 4d); a low-mass and old star (HD 208313, Fig. 4e); and another star outside the limits of the models, this time in the region of low-mass and old stars (HD 94518, Fig. 4f).

The star HD 26767 is known to be a member of the Hyades cluster, of 625 Myr, and has been studied in several works in the past decades. Other stars either very young or outside the lower border of the models have been identified as members of the Hyades, the Ursa Major ($\sim 500 \text{ Myr}$), or the Pleiades (20–150 Myr) moving groups, or even classified as possible subdwarfs. In the case of old stars outside the model limits, they are likely low-mass stars with age no older than the age of the Universe (13.8 Gyr, Komatsu et al. 2011).

Table 7 lists the derived masses and ages, together with the parameters used to compute the luminosities. The uncertainties were estimated taking into account the error propagation of the photospheric parameters and of the luminosity, using $\sigma(\pi)$ from Hipparcos, and adopting $\sigma(V) = 0.01$ and $\sigma(BC) = 0.005$. In view of the asymmetric distribution of the isochrones on the HR diagram, the table shows the lower and the upper uncertainties on age.

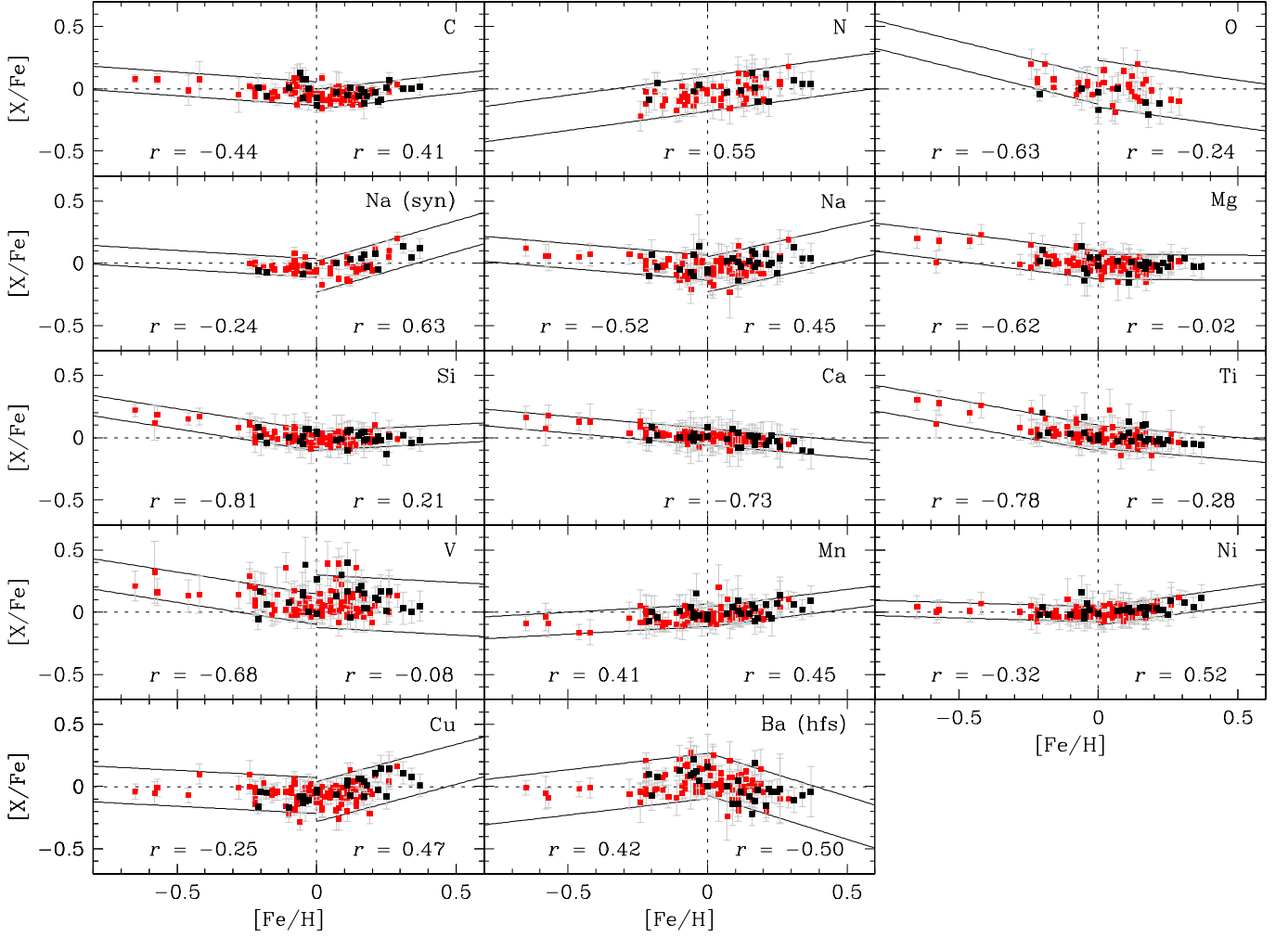


Fig. 5. Abundance ratios as a function of metallicity for our sample of 120 dwarf stars of the thin disc population. Stars with planets are represented by black symbols. For sodium, the abundance ratios from both spectral synthesis and equivalent widths determination are plotted. The 95% confidence intervals (solid lines) around linear regressions, and their respective correlation coefficients (r) are also shown. The linear regressions were derived either for $[\text{Fe}/\text{H}] \leq 0$, $[\text{Fe}/\text{H}] \geq 0$, or for the whole metallicity range, depending on which one has the more significant slope.

4.2. Kinematic properties

In the same way as in Paper 1, we grouped our stars according to their main population membership by computing the probability that a given star belongs to the Galactic thin disc, thick disc, halo, or to transition a population. First, using equations of Johnson & Soderblom (1987), we computed the space-velocity components U_{LSR} , V_{LSR} , and W_{LSR} with respect to the Local Standard of Rest (LSR) using parallaxes and proper motions from the new reduction of Hipparcos, and radial velocities from the ELODIE archive, from the Simbad database, and from Holmberg et al. (2007). For the Sun, we adopted $U_{\text{LSR}} = 10.0$, $V_{\text{LSR}} = 5.3$, and $W_{\text{LSR}} = 7.2 \text{ km s}^{-1}$ (Dehnen & Binney 1998). Then, employing the equations of Reddy et al. (2006), we computed the probability that a star belongs to one of the three populations. A probability P_{thin} , P_{thick} , or P_{halo} greater than or equal to 70% classifies the star as a thin, thick, or an halo member, respectively. If the probability is in-between, the star is classified as belonging either to the thin/thick or to the thick/halo transition group.

Our sample of 309 stars contains 281 thin-disc (out of which 120 dwarfs, 25 subgiants, and 136 giants), and 16 thick-disc (10 dwarfs, 2 subgiants, and 4 giants) population members. None of them belongs to the halo, and 13 (10 dwarfs, 2 subgiants, and 1 giant) belong to a thin/thick transition population. The membership of each star is indicated in Table 7.

5. Results and discussion

5.1. Abundance trends with metallicity

The $[\text{X}/\text{Fe}]$ abundance ratios as a function of metallicity are plotted in Figs. 5, 6, and 7 for dwarfs, subgiants, and giants, respectively. Since most of our sample stars belong to the thin disc, for homogeneity, only these stars were used in the abundance analysis. They are all listed in the tables, but only thin-disc members are displayed in the figures. Besides iron, titanium is the only element in our study having spectral lines of both neutral and singly ionized atoms. We have found no significant difference between Ti I and Ti II , hence we adopted an average value of all lines together.

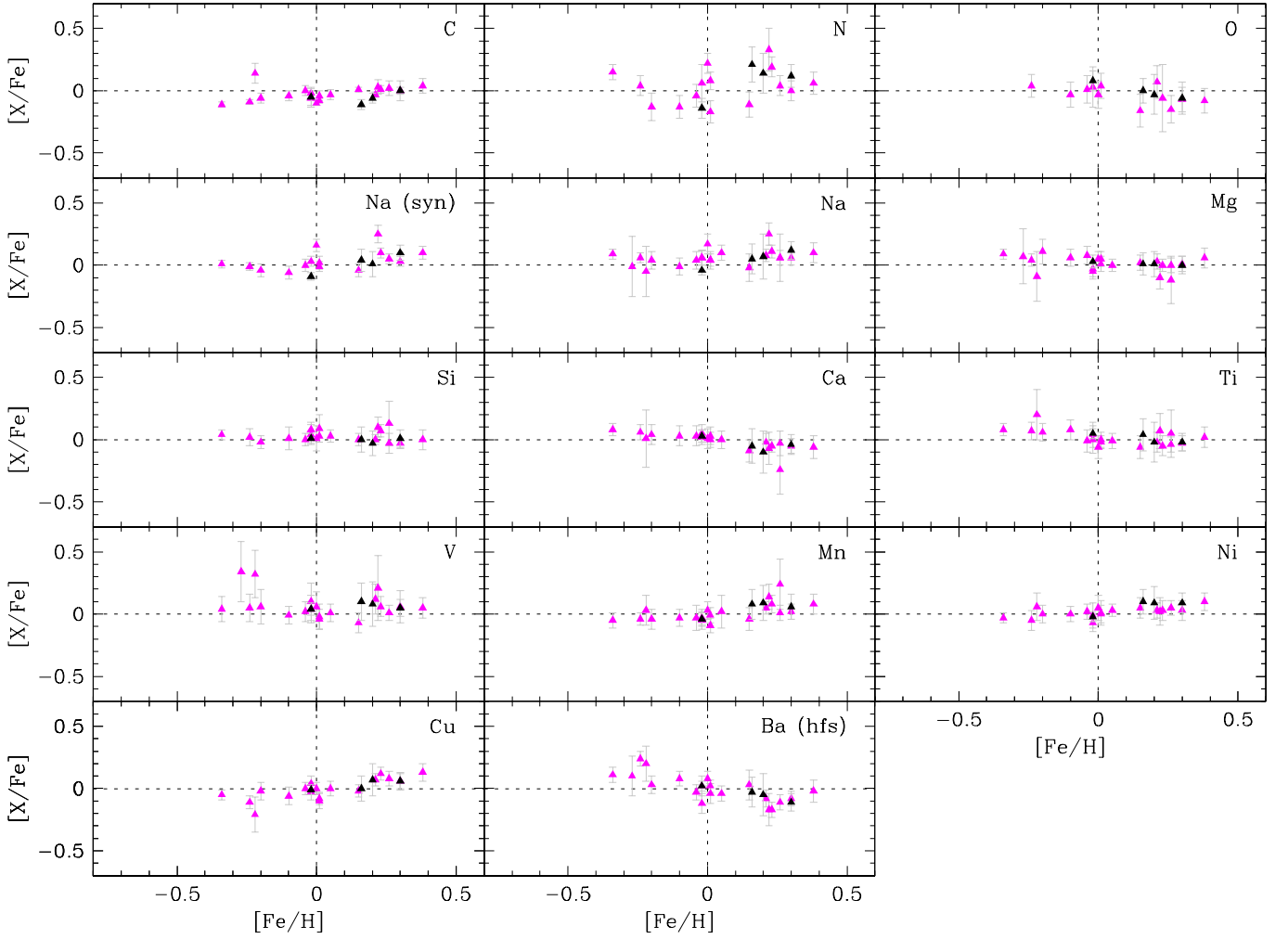


Fig. 6. The same as Fig. 5 but showing the abundance ratios of 25 subgiant stars of the thin disc population.

Despite the small number of metal-poor ($[\text{Fe}/\text{H}] < -0.3$ dex) or metal-rich ($[\text{Fe}/\text{H}] > 0.3$ dex) stars in this sample, the trends of the abundance ratios with metallicity are in good agreement with those published in the literature concerning the nucleosynthetic origin of the elements and the evolution of their abundances with time. Regarding the abundance trends for dwarfs see, e.g., Adibekyan et al. (2012b) and Kang et al. (2011). For giant stars see, e.g., Takeda et al. (2008). The abundance trends for subgiants are very similar to those for dwarfs for all the investigated elements. A few cases concerning the abundances of the three subsamples deserve particular attention, and we discuss them in the following paragraphs.

There are systematic differences in the abundance ratios of carbon, nitrogen, and sodium when the subsamples of dwarfs, subgiants, and giants are compared with each other: in the range of solar metallicity (from -0.1 to 0.1 dex) giant stars are underabundant in $[\text{C}/\text{Fe}]$ by -0.17 ± 0.07 dex, and overabundant in $[\text{N}/\text{Fe}]$ by 0.31 ± 0.10 dex and in $[\text{Na}/\text{Fe}]$ by 0.16 ± 0.08 dex. The abundance trends for these elements confirm our previous result for carbon discussed in Paper 1, and agree with the results of Takeda et al. (2008) for sodium and carbon. Concerning oxygen, we found $[\text{O}/\text{Fe}] = 0.07 \pm 0.07$ dex in the solar metallicity range. Therefore, we do not confirm the oxygen deficiency found by Takeda et al. (2008), who used the forbidden $[\text{O I}]$ line at 5577 \AA . Their oxygen abundances were in any case proba-

bly underestimated as affirmed by the authors. Our results also agree with those of Liu et al. (2010), who found that $[\text{C}/\text{Fe}]$ is depleted by 0.13 dex, $[\text{Na}/\text{Fe}]$ is overabundant by 0.1 dex, and $[\text{O}/\text{Fe}]$ was not altered after the first dredge-up. From a theoretical point of view, changes in the surface abundances of evolved stars is expected for C and N, and unexpected for O according to quantitative predictions made by Iben (1991).

A commonly used explanation for such systematic differences is based on the effect of mixing processes that dredge up C-poor and N- and Na-rich material (produced by CN and NeNa cycles) to the surface of evolved stars. On the other hand, the use of spectral lines contaminated by blends is also a possibility. In order to test this, we derived the sodium abundances using the two techniques described in Sect. 3.2, from the equivalent widths and from spectral synthesis. The available Na lines in our spectral coverage are affected by C_2 and CN molecular bands. Performing spectral synthesis allows the inclusion of the already derived C and N abundances and, therefore, to account for the presence of such bands. However, doing so, the $[\text{Na}/\text{Fe}]$ overabundance in giants is only slightly reduced, not enough to cancel out the larger systematic difference with respect to dwarfs, favoring the mixing-process hypothesis. Another result that favors this hypothesis is that $[\text{C}/\text{Fe}]$, $[\text{N}/\text{Fe}]$, and $[\text{Na}/\text{Fe}]$ have a trend with mass: a negative trend with increasing mass in the case of carbon, and positive ones for nitrogen and sodium (see

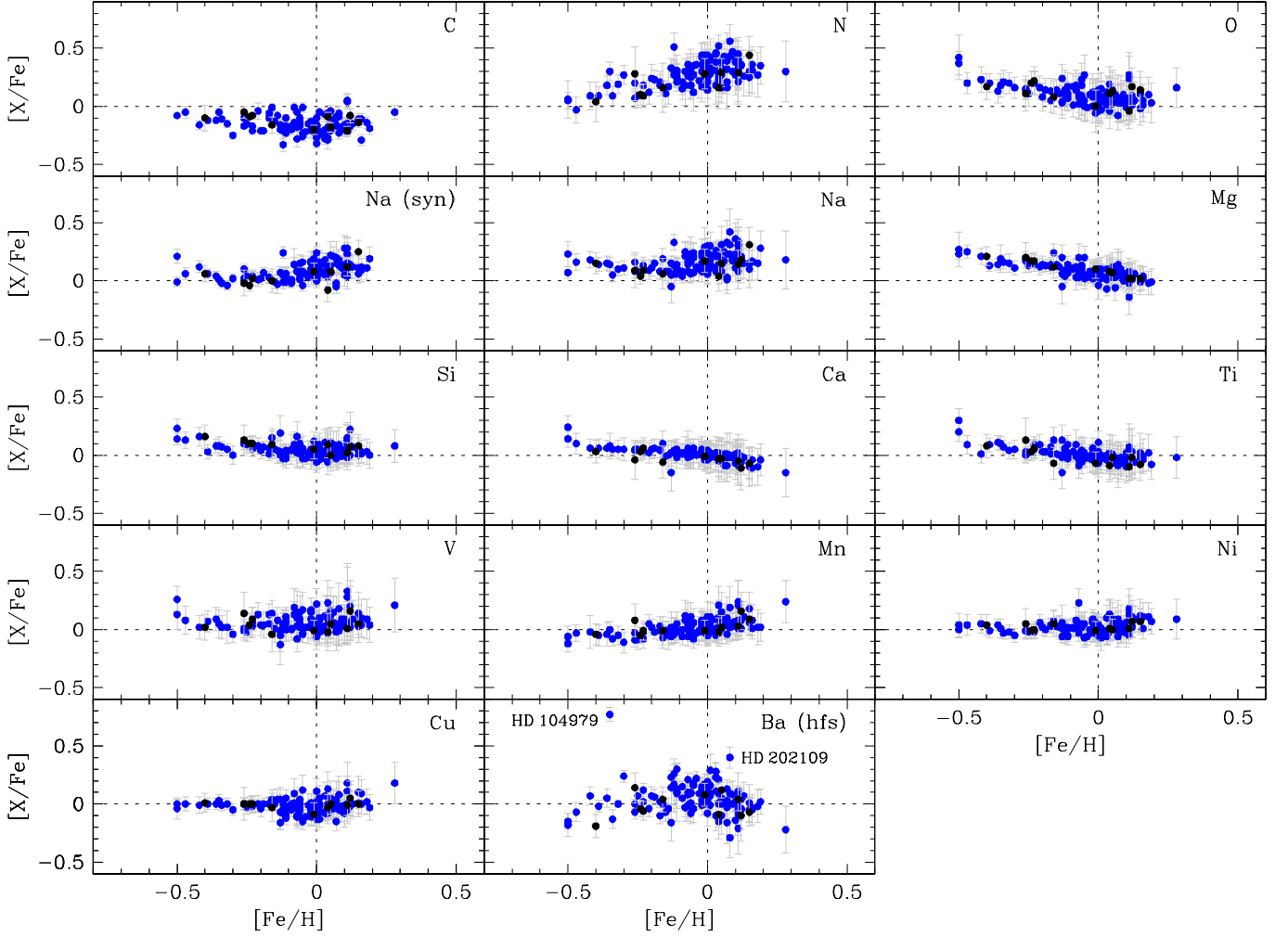


Fig. 7. The same as Fig. 5 but showing the abundance ratios of 136 giant stars of the thin disc population. The stars indicated are discussed in Sect.5.1.1.

Fig. 8). More massive stars have evolved faster and, therefore, have become C-poorer and N- and Na-rich than stars with masses close to the solar value. The oxygen abundances remain constant and independent of mass, supporting the above discussion.

The nitrogen abundances of our giant stars show a clear dependence on the effective temperature (see Fig. 9, top right panel). One possibility is that this dependence is related to the continuum definition when using the CN molecular band. In this case, the reader would ask if the trend in $[N/Fe]$ vs. $[Fe/H]$ is also related to this dependence on T_{eff} , due to a bad continuum definition. However, if we limit the effective temperature within the almost flat region seen in the $[N/Fe]$ vs. T_{eff} plane, from about 4600 to 5000 K, the trend of $[N/Fe]$ with metallicity still remains. Moreover, the effective temperature of our sample of giants increases with increasing mass, i.e., it seems that more evolved stars have higher temperatures. Therefore, we believe that the $[N/Fe]$ dependence on T_{eff} is probably related to evolution effects instead of to bad continuum definition.

Concerning the carbon abundances in dwarf stars, our result is in line with those of Delgado Mena et al. (2010) in the range of solar metallicities. They found, however, a steeper trend in $[C/Fe]$ vs. $[Fe/H]$ in the range of metal-poor stars, and practically a flat distribution of metal-rich dwarfs. On the other

hand, González Hernández et al. (2010, 2013b) derived $[C/Fe]$ ratios continuously decreasing with increasing $[Fe/H]$ in the whole range of metallicities for their sample of dwarfs and solar analogs.

For the nitrogen abundances of dwarf stars, we derived a slope of 0.31 ± 0.06 in the $[N/Fe]$ vs. $[Fe/H]$ plane for dwarfs with and without planets fitted together. This is quite steeper than the one derived by Ecuillon et al. (2004) for their sample of solar type stars with and without planets (0.10 ± 0.05) based on the NH band at 3360 Å. We checked whether our $[N/Fe]$ correlates with the effective temperature or the surface gravity, and no significant trend is observed in both cases. However, it seems that our dwarf stars with temperature higher than the solar value either have $[N/Fe]$ close to zero or are slightly overabundant, whereas those cooler than the Sun are slightly underabundant (see Fig. 9, top left panel). By performing the same fit in the $[N/Fe]$ vs. $[Fe/H]$ plane but only to stars with $T_{\text{eff}} < 5800$ K we derive a slope of 0.28 ± 0.06 , a value that is less steeper but still significantly high.

The decreasing $[O/Fe]$ with increasing metallicity observed for our sample of dwarfs agrees with the trends derived by Delgado Mena et al. (2010) and by González Hernández et al. (2010, 2013b), and also with the recent results by

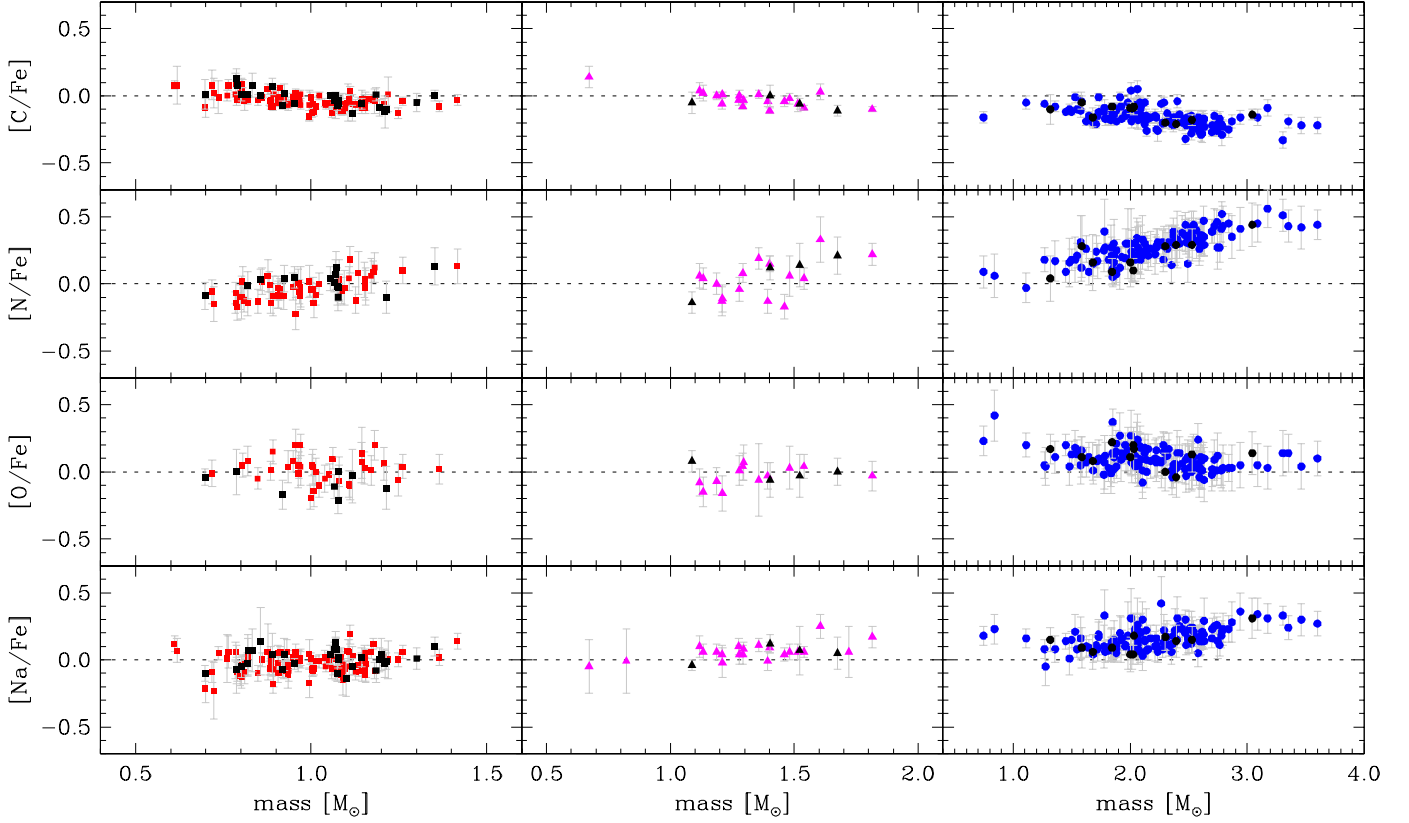


Fig. 8. Abundance ratios of C, N, O, and Na as a function of mass for our sample of dwarfs (left panels), subgiants (middle panels), and giants (right panels). Stars with planets are represented by black symbols.

Bertran de Lis et al. (2015) for the O abundances based on the O I $\lambda 6158.17$ and [O I] $\lambda 6300.30$ atomic lines.

The distributions of $[X/H]$ are shifted towards higher abundances (see Fig. 13) due to the metal-rich nature of stars hosting giant planets as already known and discussed in the literature (see, e.g., Neves et al. 2009; Adibekyan et al. 2012b). The exceptions in the current study are oxygen and barium, which $[X/H]$ abundances show no clear enrichment in giant planet hosts (see discussion in Sect. 6). In other words, most of these elements follows the same behavior of iron and are, for some reason, also linked to the planetary formation process. It is worth noting that only stars with giant planets (mass ≥ 50 Earth masses) were considered and compared with only stars for which no giant planet has been detected. We conducted an exhaustive search in the literature in order to classify each star and create these two subsamples. They are identified in the remarks column of Table 7, together with the respective reference. In addition, we note that we performed this comparison only for dwarf stars of the thin disc population. Evolved stars are normally not included in the surveys of planet search, because they are well known for their intrinsic radial-velocity variation due to pulsation and/or jitter (distortion in the observed signal caused by stellar magnetic activity). Subgiant stars could be added to the subsample of dwarfs, but we preferred to keep the homogeneity.

In order to quantify the observed trends with metallicity, we fitted linear regressions in the range of stars metal-poorer or metal-richer than the Sun, or in the whole range of metallicity, depending on which one provides a higher correlation. The abundance ratios were then subtracted by the predictions of these linear fits trying to remove (or at least minimize) the effects of the chemical evolution of the Galaxy's thin disc. The abundances

corrected from such effects are used and discussed in Sect. 5.3, where we derive the trends with condensation temperature of the elements.

5.1.1. Chemically peculiar stars

Most of the dwarf and subgiant stars plotted in Figs. 5 and 6 follow the abundance trends with metallicity. A particular exception seems to be the vanadium abundance ratios for some of them. Such stars have $[V/Fe]$ higher than what is expected for their metallicity. By plotting the abundance ratios of the elements as a function of the other stellar parameters, we noticed that there is a systematic positive trend of $[V/Fe]$ as a function of the effective temperature for $T_{\text{eff}} \geq 6000$ K for our sample of dwarfs (see Fig. 9, bottom left panel). For this reason, in the following sections we discuss the results obtained by including or excluding the vanadium abundances of stars with temperature higher than this limit. No clear trend with temperature for the other elements is observed, and of the abundance ratios with the other stellar parameters (except age) neither. This is the case at least for dwarfs and subgiants, because the elemental abundances in giants may have been affected by stellar evolution (see discussion in Sect. 5.1).

Concerning the chemical peculiarity of giant stars, two of our sample stars deserve special given their position in the $[Ba/Fe]$ vs. $[Fe/H]$ diagram of Fig. 7. Both HD 104979 and HD 202109 appear enriched in barium compared to other giants with the same metallicity. Williams (1971) derived a $[Ba/Fe] = 1.1$ dex for HD 104979 and first suggested it to be a Ba II

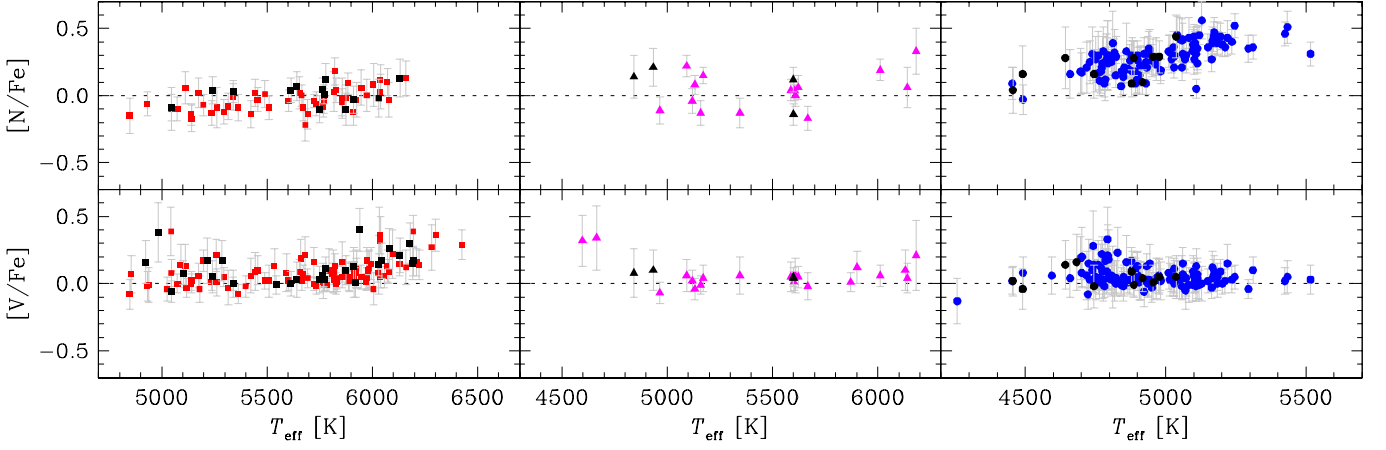


Fig. 9. $[N/Fe]$ and $[V/Fe]$ as a function of the effective temperature for our sample of dwarfs (left panels), subgiants (middle panels), and giants (right panels). Stars with planets are represented by black symbols.

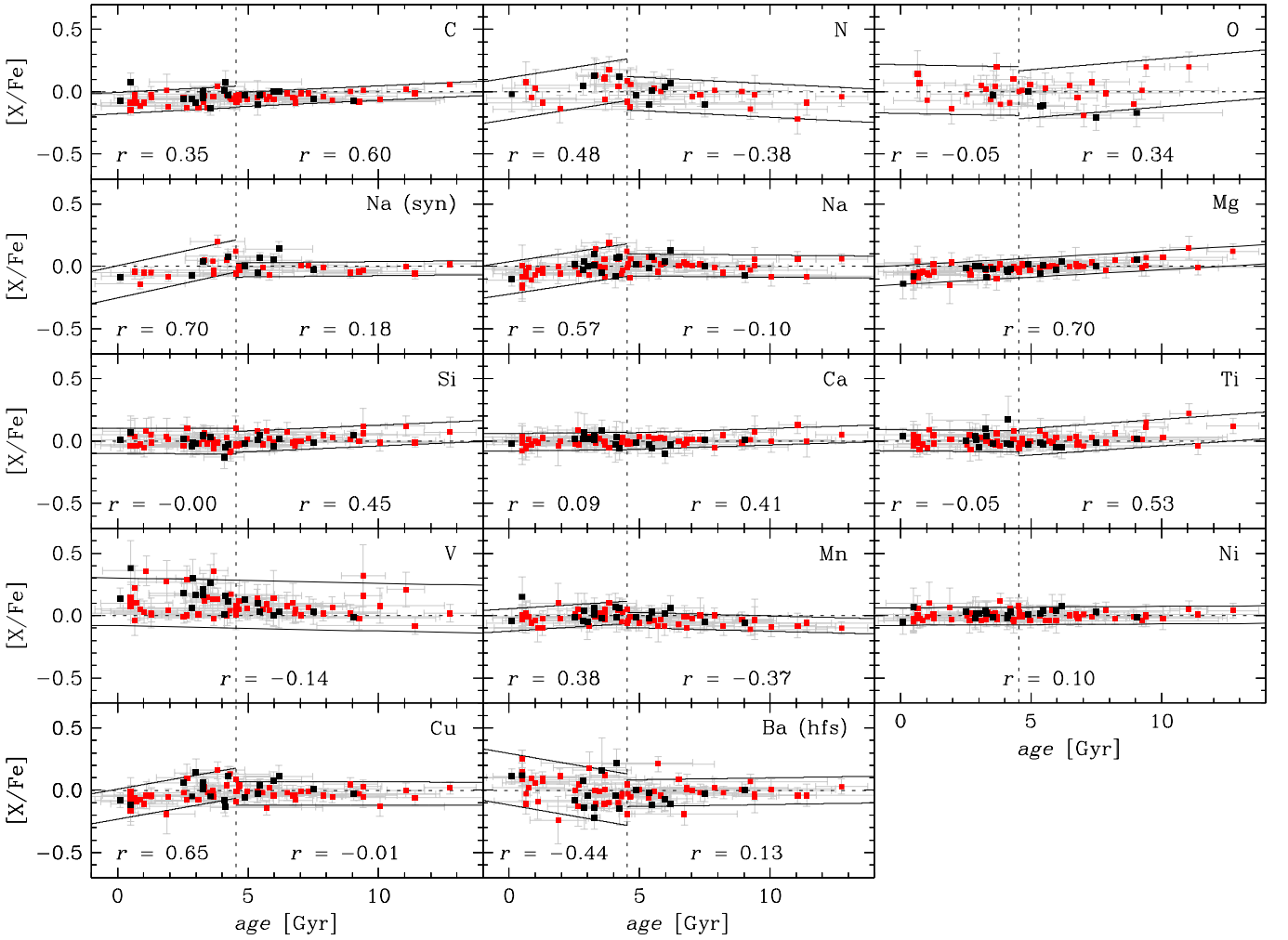


Fig. 10. Abundance ratios as a function of age for our subsample of 120 dwarf stars of the thin disc population. Stars with planets are indicated by black symbols. For sodium, the abundance ratios from both equivalent widths and spectral synthesis determination are plotted. The vertical dashed line indicates the adopted solar age (4.53 Gyr). The 95% confidence intervals (solid lines) around linear regressions, and their respective correlation coefficients (r) are also shown. The linear regressions were derived either for age ≤ 4.53 Gyr, age ≥ 4.53 Gyr, or for the whole range in age, depending on which one has the more significant slope.

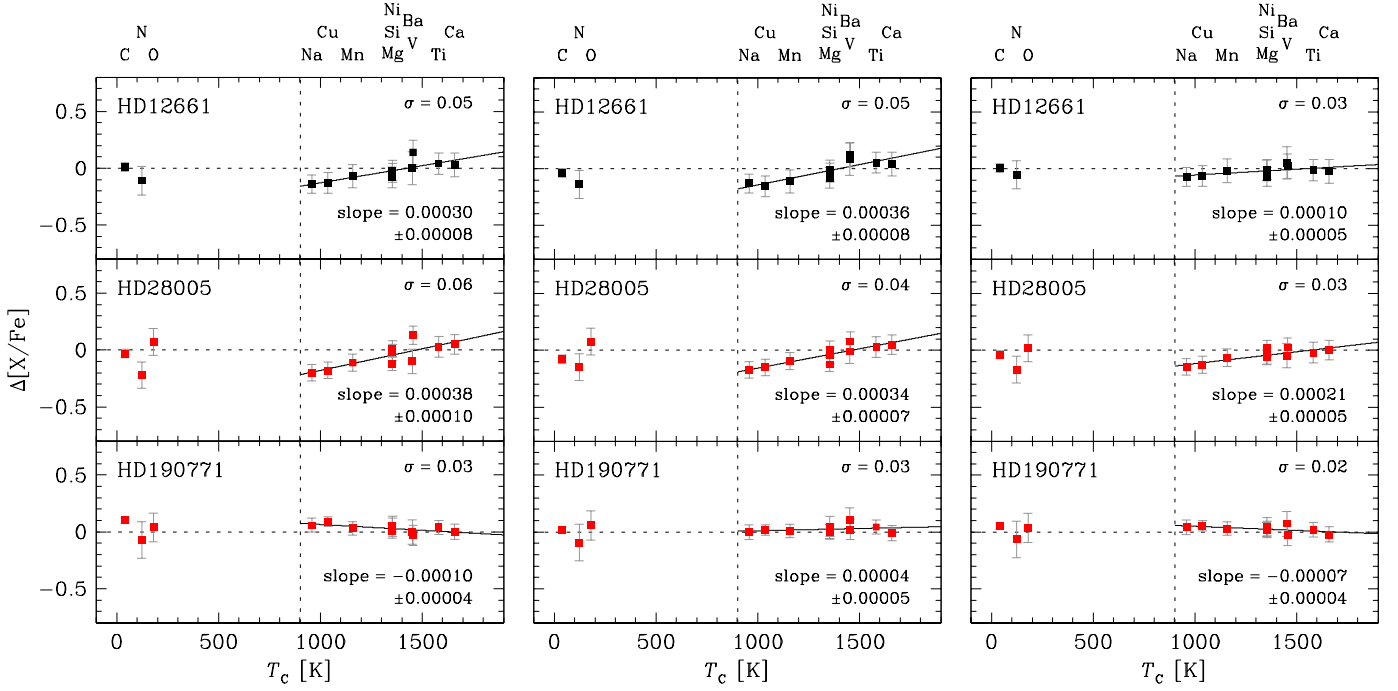


Fig. 11. Abundance differences $[X/Fe]_{\text{Sun}} - [X/Fe]_{\text{stars}}$ as a function of the condensation temperature of the elements for some of our dwarf stars of the thin disc population. We show the trends before (left panels) and after applying the corrections for the Galactic chemical evolution effects based on age (middle panels) and on metallicity (right panels). The standard deviations of the linear regressions (solid lines) for $T_C > 900$ K and their respective slopes are also shown. The planet host star is indicated by black symbols.

star². More recent works have confirmed the barium overabundance for this star, namely $[Ba/Fe] = 0.93 \pm 0.10$ dex (Zács 1994) and $[Ba/Fe] = 0.54 \pm 0.31$ dex (Smiljanic et al. 2007), both in agreement with our determination of $[Ba/Fe] = 0.77 \pm 0.06$ dex. The barium star nature of HD 202109 was first suggested by Chromey et al. (1969), who measured $[Ba/Fe] = 0.8 \pm 0.3$ dex, and afterward classified as mild (marginal enriched) barium stars: $[Ba/Fe] = 0.41 \pm 0.13$ dex by Zács (1994), and $[Ba/Fe] = 0.31 \pm 0.26$ dex by Smiljanic et al. (2007). We derived $[Ba/Fe] = 0.40 \pm 0.09$ dex, a result that agree with the mild barium star classification.

5.2. Abundance trends with age

Figure 10 shows the $[X/Fe]$ abundance ratios as a function of age for the subsample of dwarf stars of the thin disc population. Similarly to what is described in Sect. 5.1 in the case of the metallicity, we also quantified the observed trends with age by fitting linear regressions in the range of stars younger or older than the Sun, or in the whole range of age, depending on which one provides a higher correlation. Again, the abundance ratios were subtracted by the predictions of these linear fits in order to remove (or at least minimize), using another approach, the effects of the chemical evolution of the Galaxy. The abundances corrected from such effects are used and discussed in Sect. 5.3,

² A Ba II star originates in the following scenario: when the more massive component of a binary system evolves as a thermally pulsing asymptotic giant branch star, the material produced in the He-burning envelope, enriched in s-process elements, is dredged up to the surface and then accreted by the companion by wind mass transfer. The initially more massive star finishes as a white dwarf whereas the companion becomes a primary barium star.

where we derive the trends with condensation temperature of the elements.

Depending on the position of the star in the HR diagram, the errors in age may be quite high, and the age determination is thus less reliable. By means of the distribution of the uncertainties on this parameter, we set a 2σ confidence limit up to which about 95% of the stars are found to have errors smaller than that limit, namely ~ 4 Gyr. Hence, only stars with $\sigma(\text{age}) < 4$ Gyr was considered in the analysis.

5.3. Abundance trends with condensation temperature

During the last few years, several works have investigated the relation between the stellar chemical abundances and the condensation temperature (T_C) of the elements in stars with and without planets. Aiming to minimize systematic errors, the abundance difference between the Sun and other stars, $\Delta[X/Fe]$, has been used, where the solar abundances are derived from, e.g., a Moon's spectrum.

On the one hand, it has been suggested that the observed trends of $\Delta[X/Fe]$ as a function of T_C may have some relation with the planetary formation, in particular, with the formation of terrestrial planets (see the review performed by Ramirez et al. 2010). On the other hand, other authors argued that this kind of relation practically vanishes after removing the Galactic chemical evolution effects (see González Hernández et al. 2013b, and references therein). Indeed, positive slopes in these diagrams may be the result of having higher abundances of less refractory elements, such as Na and Cu, with respect to more refractory ones, such as Ti and Ca. In Fig. 5, both $[Ti/Fe]$ and $[Ca/Fe]$ have a slight decrease with increasing metallicity whereas $[Na/Fe]$ and $[Cu/Fe]$ clearly increase for higher metallicities.

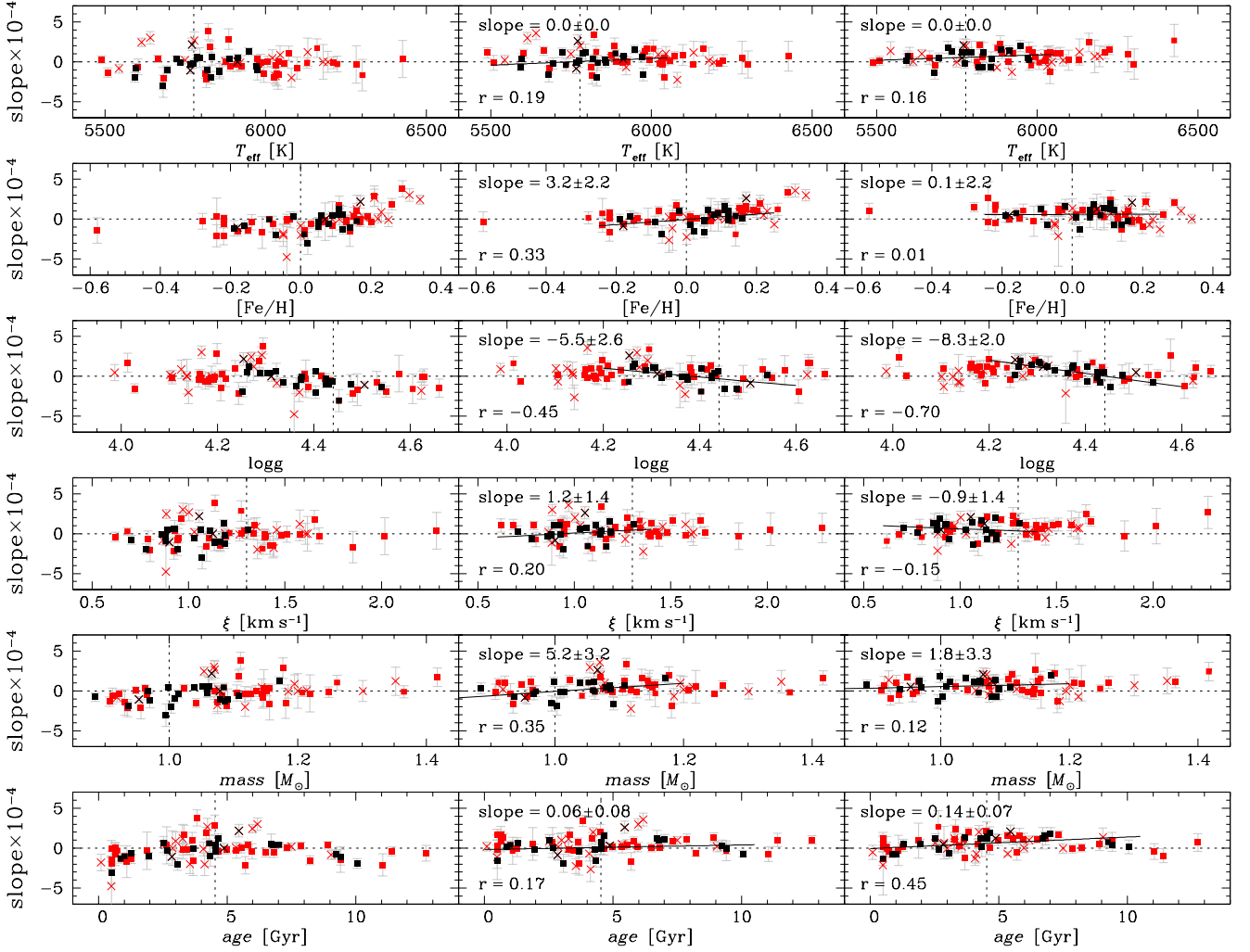


Fig. 12. Slope of the regressions computed in the diagrams $\Delta[X/Fe]$ vs. T_C (Fig. 11) plotted as a function of the derived stellar parameters. We show possible trends before (left panels) and after applying the corrections for the Galactic chemical evolution effects based on age (middle panels) and on metallicity (right panels). Dwarf stars of the thin disc population are separated in solar analogs (red symbols) and non-solar analogs (black symbols). Stars with planets are indicated by crosses. The slopes of linear regressions (solid lines) applied to the solar analogs and their respective correlation coefficients (r) are also shown.

In particular, some of the studies discussed in the papers above consider only solar twins ($T_{\text{eff}} = 5777 \pm 100$ K, $[Fe/H] = 0.0 \pm 0.1$ dex, $\log g = 4.44 \pm 0.10$ dex) or solar analogs ($T_{\text{eff}} = 5777 \pm 200$ K, $[Fe/H] = 0.0 \pm 0.2$ dex, $\log g = 4.44 \pm 0.20$ dex) in their analysis. Recently, Adibekyan et al. (2014) have published the results of their study in which they searched for correlations of the $\Delta[X/Fe]$ vs. T_C trends with some stellar and orbital parameters. After correcting the abundances from the Galactic chemical evolution effects, they found that the observed trends correlate with age and anticorrelate with the surface gravity, and possibly with the mean Galactocentric distance, and that the correlations (or anticorrelations) are even steeper and more evident if only solar analogs are plotted.

Here we also investigate the relations involving $\Delta[X/Fe]$ as a function of the condensation temperature of the elements (to compute $[X/Fe]_{\text{Sun}}$, we used the solar abundances derived from the spectrum of the sunlight reflected by the Moon). First, we fitted linear regressions for elements with $T_C > 900$ K, a limit normally used to distinguish refractory from volatiles. Values of T_C were taken from Lodders et al. (2009). In order to account for any effects that the Galactic chemical evolution may have on

the observed trends, we applied the corrections based on both metallicity and age, as described previously. Figure 11 shows a few examples. Table 8, available in electronic form at the CDS, lists the slopes of the linear regressions and the respective standard deviations for all dwarfs. Only dwarf stars were used in this analysis because their abundances are normally not affected by stellar evolution. The table contains the slopes and their uncertainties, the correlation coefficients, and the standard deviations of the regressions before and after applying the corrections for the Galactic chemical evolution effects based on age and on metallicity.

We then plot (Fig. 12) the respective slopes as a function of the stellar parameters T_{eff} , $[Fe/H]$, $\log g$, ξ , mass, and age. In this figure, solar analogs are distinguished from non-solar analogs, and stars with planets from those without planets. Regarding the sample of solar analogs, the figure shows: *i*) a marginal correlation with metallicity (in the sense that metal-rich stars have more positive slopes) and with mass after removing the effects of chemical evolution based on age; however, these correlations completely disappear if the correction is based on metallicity; *ii*) a clear anticorrelation with the surface gravity in both sce-

narios of Galactic chemical evolution correction; *iii*) a marginal correlation with age, slightly steeper after applying the correction based on metallicity. The directions of these correlations agree with those reported by Adibekyan et al. (2014). We cannot check the T_C trends with Galactocentric distance because we only have solar neighborhood stars (distance to the Sun < 100 pc). Concerning the relation with the presence of planets, the small number of planet hosts in our sample of solar analogs prevents us from any conclusions.

By excluding from the analysis the vanadium abundances of stars with $T_{\text{eff}} \gtrsim 6000$ K, the correlations and anticorrelations obtained above are still the same, specially because this limit is already imposed when only solar analogs are used.

6. Statistical analysis

We have used a number of statistical methods (see Breiman et al. 1984) to explore the multivariate properties of our sample. We are interested in uncovering significant differences in the stellar properties for stars with and without a known giant planet. Hereafter we will use the indices 1 and 0 to distinguish these two samples, respectively. Moreover, the sample of dwarf stars will be prefixed by the letter “d”. Thus, samples d1 and d0 stand for dwarfs with and without a known giant planet, respectively. The analysis and the following discussion is restricted to the dwarfs because their sample is thought to be less affected by an observation bias.

6.1. Abundance distributions

We compare the abundance distributions between the samples d0 (red) and d1 (blue) in Fig. 13. The boxes and whiskers summarize graphically percentiles of these abundance distributions. Particularly, the middle line inside each box marks the median for that distribution, whereas the upper and lower edge of the box indicate the interquartile range. We applied a 2σ clipping in the abundance data of each single element in order to get rid of outliers in the abundance space. Panel (a) shows the comparison for all dwarf stars after applying the sigma clipping, while panel (b) restricts the comparison to those stars having $-0.25 \leq [\text{Fe}/\text{H}] < +0.35$ (a range in common between the subsamples of stars with and without planets). Both comparisons depict that dwarf stars with giant planets (d1) have generally larger abundances in nearly all elements compared to dwarfs without giant planets (d0). We note that vanadium seems to be exceptionally abundant in d1 stars, whereas no significant difference is seen between d1 and d0 for the oxygen and barium abundances. Concerning vanadium, the overabundance of d1 with respect to d0 does not change if only stars with $T_{\text{eff}} \lesssim 6000$ K are used.

We used the Welch’s t-test to quantitatively assess whether the means of these distributions are significantly different from one another. Table 1 gives the test statistics for stars having $-0.25 \leq [\text{Fe}/\text{H}] < +0.35$, after applying 2σ clipping. Some p -values are very low (< 0.001), reinforcing the visual comparison provided by Fig. 13. The mean of the abundance distribution of all elements, but O and Ba, are higher in d1 stars, compared to d0 stars. Oxygen abundances are not very well represented in our sample, and only 32 d0 and 4 d1 stars have measured O abundance; this could be one of the reasons for why the t-test gave a large p -value for the O abundance distribution comparison. Notwithstanding, it is highly interesting, although not clear, why Ba is not particularly more abundant in d1 stars.

The t-tests described above can only be applied to the abundance distribution of a single element at a time. They can pin-

point elements that are particularly more or less abundant in one of the tested distributions. To use the information encoded in the whole abundance space, we also applied a multivariate analysis of variance (MANOVA) to assess for the significance of differences in the multivariate means (that is, the location of samples 0 and 1 in the abundance space). According to this MANOVA, we can reject the null hypothesis that the d0 and d1 samples have similar locations in the abundance space ($p = 0.006$).

6.2. Abundance difference per metallicity bin

We have also considered a different approach to disentangle the effects of the chemical evolution of the Galaxy from the metallicity–giant planet connection. We have defined a crude abundance quantity $\mathcal{Z} = [\text{Mg}/\text{H}] + [\text{Si}/\text{H}] + [\text{Ca}/\text{H}] + [\text{Ti}/\text{H}] + [\text{V}/\text{H}] + [\text{Mn}/\text{H}] + [\text{Ni}/\text{H}] + [\text{Cu}/\text{H}] + [\text{Ba}/\text{H}]$. \mathcal{Z} does not have an exact physical meaning, on account of the sum of unscaled log abundances, but it can serve as enrichment index for the purpose of this analysis. For instance, it is clear that \mathcal{Z} and $[\text{Fe}/\text{H}]$ should be correlated as a result of the Galactic chemical evolution. This index could only be defined for those stars having a complete set of abundances of the elements Mg to Ba, including Fe. CNO and Na abundances were not included in the \mathcal{Z} definition because this would lower substantially the final number of stars having a complete set of abundance measurements.

The index was used in a linear model of the type

$$\mathcal{Z} = \hat{\beta}_0 + \hat{\beta}_1[\text{Fe}/\text{H}] + \epsilon, \quad (1)$$

fitted by least squares to the d0 stars. The residuals of the fit are given by ϵ for each star. Following this, we calculated the residuals of the d1 stars with respect to the same linear model fitted to the d0 stars. A Welch’s t-test applied to these residual distributions indicate that the difference in their means are significant (a p -value $p = 0.0023$), with $\bar{\epsilon}_{\text{d1}} - \bar{\epsilon}_{\text{d0}} = 0.16 \pm 0.10$. That is, for a given $[\text{Fe}/\text{H}]$, d1 stars have generally larger \mathcal{Z} indices than d0 stars. If we can consider the d0 stars as a “null hypothesis” population, for which the elemental abundances only reflect the Galactic chemical evolution, the residuals of \mathcal{Z} for the d1 stars using the linear model in Eq. 1 should have no chemical evolution bias. Again, if we calculate \mathcal{Z} excluding $[\text{V}/\text{H}]$, this result practically does not change (the new p -value would be $p = 0.0026$). On the other hand, if \mathcal{Z} is calculated excluding the $[\text{Ba}/\text{H}]$ abundance ratios, we obtain $p = 0.0005$ and $\bar{\epsilon}_{\text{d1}} - \bar{\epsilon}_{\text{d0}} = 0.22 \pm 0.12$, i.e., the difference between the d0 and d1 populations is even larger.

We defined \mathcal{Z} by mixing elements with different nucleosynthetic origins, which might veil the real difference in abundance between stars with and without planets. However, the mean $[\text{X}/\text{H}]$ distributions for α (Mg, Si, Ca, Ti) and for iron-peak (V, Cr, Mn, Co, Ni) elements in stars hosting giant planets are very similar, as reported by Mata Sánchez et al. (2014). Indeed, if we calculate \mathcal{Z} for α elements only we obtain $\bar{\epsilon}_{\text{d1}} - \bar{\epsilon}_{\text{d0}} = 0.08 \pm 0.06$, whereas for our iron-peak elements (V, Mn, Ni) only we have $\bar{\epsilon}_{\text{d1}} - \bar{\epsilon}_{\text{d0}} = 0.10 \pm 0.06$. For stars without planets, the $[\text{X}/\text{H}]$ distributions are also very similar, having a maximum abundance at ~ -0.1 for most species (Mata Sánchez et al. 2014). Therefore, we conclude that the mix of elements when calculating \mathcal{Z} is not a bad approach, specially because the differences that we are comparing become more significant when the abundances of all these elements are added together.

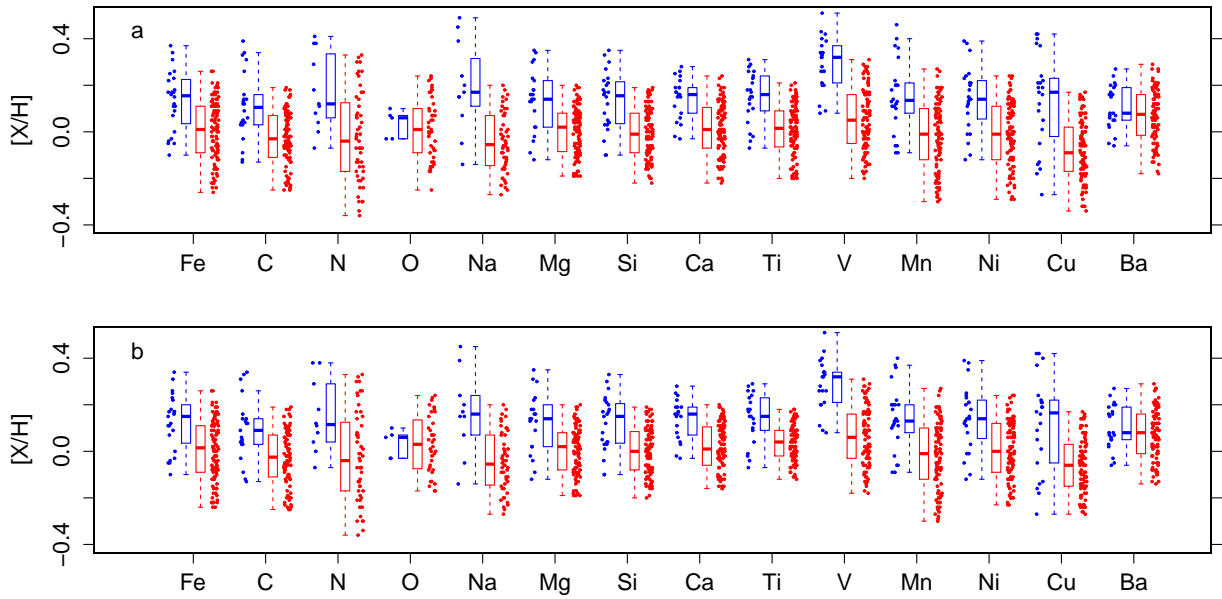


Fig. 13. Boxplot for the comparison between the elemental abundances of dwarf stars with and without planets, show in blue and red, respectively. Two sigma clipping was applied to all abundance distributions before the comparison, to avoid abundance outliers. The top panel shows the distributions for dwarfs in the $[Fe/H]$ abundance space, whereas the bottom panel restrict the comparison to those stars having $-0.25 \leq [Fe/H] < +0.35$. The original data points are shown beside each corresponding box to allow the visualization of the intrinsic scatter.

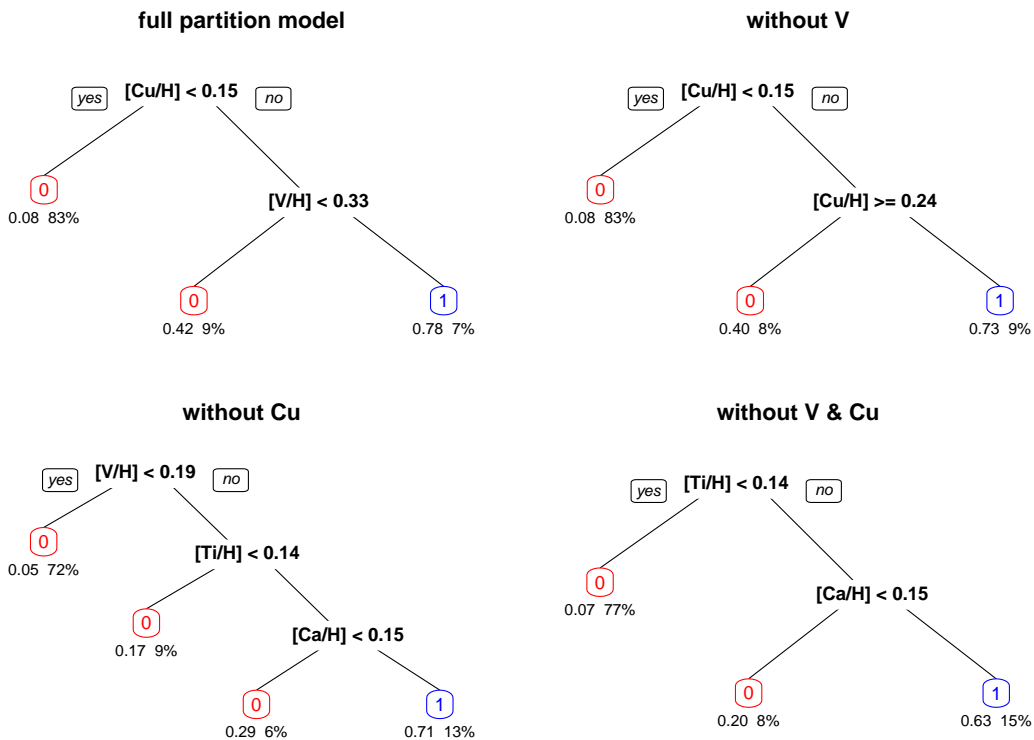


Fig. 14. Classification trees for the planet-harboring status amongst dwarf stars in our sample. The nodes are annotated with a categorical binary variable that assumes values 1 or 0 for stars with and without a giant planet, respectively. The leaves are marked with statistics of the partitioned group: fraction of d1 stars in the group (stars harboring a giant planets) and percentage of all dwarfs stars that were classified in that leaf. The top left tree is the full partition model for our sample. The other trees consider the case when two important elements are not known: V and Cu, one at a time or both.

6.3. Classification trees

Assuming the general connection between chemical abundance and the presence of a giant planet, we can extend the reasoning in using the iron abundance as an indicator of the plausibility that the star harbors a planet. To do this, we applied a classification tree to a complete set of $[X/H]$ abundances for the dwarfs in our sample. Classification trees give the optimal splitting of observations coming from different classes (or populations). In our problem, we consider two classes: stars with and without giant planets. The tree is built through recursive partitioning of the abundance space into nested groups, aiming at terminal groups having highest purity (that is, having most, if not all, of its members coming from a single class). Each classification tree has nodes, branches and terminal leaves (or group). The nodes are annotated with some property (or variable) and a splitting rule which points to a branch or the other. The leaves are usually marked with statistics of the partitioned group.

As previously explained, on account of the requirement to have a complete set of abundances, CNO and Na measurements were not used in this analysis. No sigma clipping to the abundances was used before applying the classification trees. We show in Fig. 14 four classification trees. The leaves are marked (and color-coded, for easy identification) with the most likely class of its members: 0 (red) if the star is not likely to harbor a giant planet, and 1 (blue) if the opposite holds. Two numbers are annotated below each terminal leaves, showing the fraction of d1 stars in the group (stars harboring a giant planet) and the percentage of all dwarfs stars that were classified in that leaf. Thus, the numbers 0.42 9% can be read as 9% of all dwarfs were classified in that group and 42% of them harbors a giant planet. The upper left panel gives the classification tree when we consider all elements from Mg to Ba. Although this abundance space is formed by the measurements of 10 chemical species, only two of them are needed for an optimal partition: Cu and V. Copper abundances seems to be the best single indicator of the presence of a giant planet: only 8% of the stars having $[Cu/H] < 0.15$ dex harbors a giant planet. Vanadium comes second in refining this: 78% of stars having $[Cu/H] \geq 0.15$ dex and $[V/H] \geq 0.33$ dex harbors a giant planet. The three other classification trees in Fig. 14 shows the partition model when Cu, V or both variables are not used. If vanadium is taken out of the independent variable set, the whole 10-dimensional abundance space could still be partitioned using the Cu abundances alone. The purity is somewhat lower: 73% of the stars having $0.15 \leq [Cu/H] \leq 0.24$ harbors a giant planet. If, on the other hand, we take Cu from the set of independent variables, V takes the lead as the most relevant element, followed by two more splittings using Ti and Ca. The two more meaningful (extreme) leaves give: *i*) 5% of stars having $[V/H] < 0.19$ dex harbors a giant planet; and *ii*) 71% of stars having simultaneously $[V/H] \geq 0.19$, $[Ti/H] \geq 0.14$ and $[Ca/H] \geq 0.15$ dex harbors a giant planet. Taking both Cu and V out of the set of independent variables yields a classification tree based on Ti and Ca abundances that is an exact subtree from the third case (with no Cu abundances).

6.4. Linear discriminant analysis

A similar, but more sophisticated, approach can be done using a linear discriminant analysis (LDA), which finds the linear combination of observed properties (in our case, abundances) which best separates two or more classes of objects. The result is an index, or system of indices, that may act as a linear classifier. The difference from the classification tree is that this one uses

Table 1. Probabilities of the t-test statistics and coefficients of the linear discriminant for the d0 and d1 classes.

Abundance ratio	$N(d0)$	$N(d1)$	p -value	Linear discriminant
[Fe/H]	94	23	2.39×10^{-4}	-0.87
[C/H]	86	21	5.12×10^{-4}	...
[N/H]	51	10	6.82×10^{-3}	...
[O/H]	36	5	9.21×10^{-1}	...
[Na/H]	48	10	4.92×10^{-3}	...
[Mg/H]	89	20	8.38×10^{-4}	-5.43
[Si/H]	87	23	1.43×10^{-4}	0.70
[Ca/H]	88	20	7.62×10^{-6}	-0.14
[Ti/V]	79	21	2.76×10^{-4}	8.23
[V/H]	85	21	2.03×10^{-9}	2.27
[Mn/H]	91	23	3.56×10^{-5}	-3.50
[Ni/H]	88	23	1.64×10^{-4}	5.62
[Cu/H]	81	22	6.76×10^{-4}	0.99
[Ba/H]	82	22	1.91×10^{-1}	-2.01

Notes. The second and third columns gives the number of stars in each group. The p -value gives the probability that the mean of both d0 and d1 distributions are statistically similar.

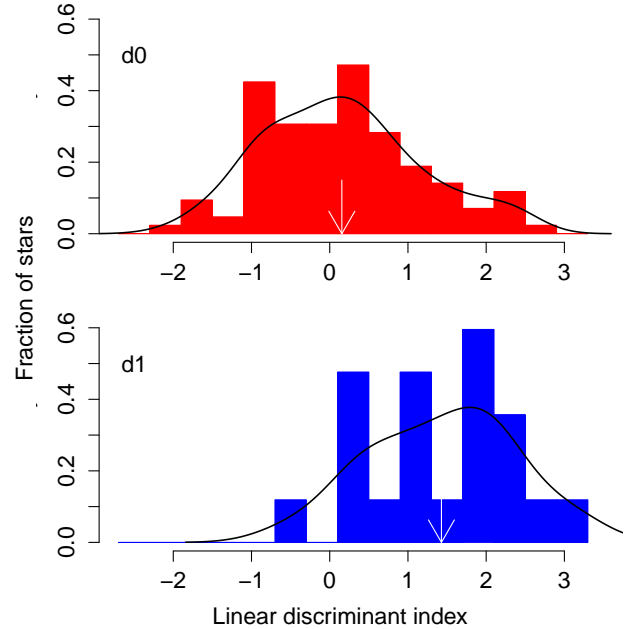


Fig. 15. Histograms of the linear discriminant indices defined in Table 1. The color code blue and red is used to indicate stars with (top panel) and without planets (bottom panel), respectively. A black line shows the kernel density function for these indices, and a white arrow marks the position of the mean in each distribution.

a hierarchical recursive splitting of single properties, aiming at classes with highest purity possible, while the LDA searches for rotations of the original multi-parametric space that leads to the best discrimination of the classes in the entire space.

We applied the LDA to the complete abundance set of Mg to Ba for dwarfs, looking for the linear combination of abundances that could better discriminate the d0 from d1 samples. The resulting linear discriminant is given in the last column of Table 1 and in Fig. 15. As explained, the LDA finds the

best linear combination of the original abundances that discriminate amongst the tested classes. The numbers in the table are the coefficients of this linear discriminant. An index formed by $-0.87[\text{Fe}/\text{H}] - 5.43[\text{Mg}/\text{H}] + \dots + 0.99[\text{Cu}/\text{H}] - 2.01[\text{Ba}/\text{H}]$ can thus be used to discriminate d0 from d1 stars. If our sample can be taken as unbiased and representative of the stellar abundances of stars with and without giant planets, we can use this discriminant index in a predictive way, when the giant planet-harboring status of the star is unknown a priori. As pointed before, the concept is similar to using a classification tree, although now we use all abundances to build a single optimizer classifier. The power of this classifier can be seen in Fig. 15, where we show the histogram of the discriminant index.

We explored all possible combinations of abundance ratios involving the elements from Mg to Ba, using the Welch's test to assess interesting pairs. After considering all possibilities, we have found that $[\text{V}/\text{Ca}]$ seems to be a good abundance ratio for discriminating dwarfs with planets: the average difference in $[\text{V}/\text{Ca}]$ between the d0 and d1 groups amounts to 0.07 dex, leading to the rejection of the null hypothesis with $p = 0.005$.

Kernel probability density functions for the relevant abundance ratio that allows the discrimination of dwarfs with and without giant planets are shown in Fig. 16. The color code is similar to that used before: blue and red for stars with and without planets, respectively. The figure shows the $[\text{V}/\text{Ca}]$ amongst dwarf stars. Although there is considerable intersection between the red and blue curves, it is both remarkable and puzzling that this abundance ratio seems to discriminate stars according to their planet-harboring status.

7. Conclusions

The inclusion in the current study of more stars, with and without detected planets, and more elements aimed to improve the work presented in Paper 1. A summary of our new results and conclusions is as follows:

- i)* the systematic differences in the abundance ratios of C, N, and Na among dwarfs, subgiants, and giants seem to confirm that mixing processes, together with cycles of nucleosynthetic reactions, do modify the abundances in the surface of evolved stars;
- ii)* such mixing processes seem, indeed, to alter the Na photospheric abundances in giant stars considering that, even tanking into account the influence of C_2 and CN molecular features, a Na overabundance is still observed;
- iii)* the slopes in the $\Delta[\text{X}/\text{Fe}]$ vs. T_{C} diagrams show a correlation with age and an anticorrelation with the surface gravity, even after accounting for the effects of the Galactic chemical evolution; these results appear only when the sample is restricted to solar-analog stars; in other words, as also pointed out by Adibekyan et al. (2014), older and more evolved stars are, in same way, connected to a lower amount of more refractory elements available for the star formation; no significant correlation with other stellar parameters, and no relation with the presence of planets are observed;
- iv)* our statistical analysis has provided the following results:
 - a)* the overabundance of other elements in dwarf stars hosting giant planets confirms the previous statement that not only iron is linked to the planetary formation process, but also C, N, Na, Mg, Si, Ca, Ti, V, Mn, Ni, and Cu;
 - b)* for O and Ba there are no significant differences between the samples of dwarfs with and without giant planets; oxygen

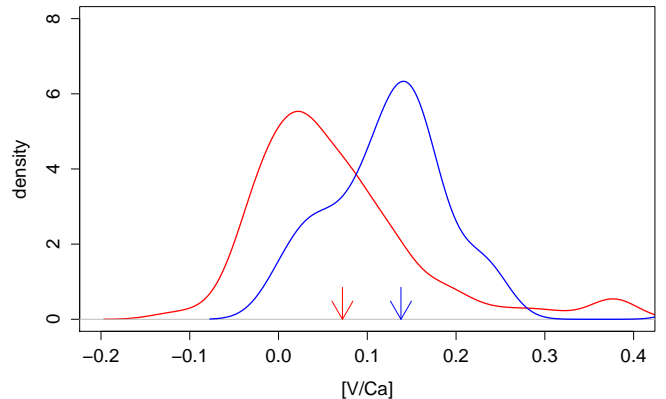


Fig. 16. Kernel probability density functions for the relevant abundance ratio, $[\text{V}/\text{Ca}]$, that allows the discrimination of dwarfs with and without giant planets. The color code blue and red is used to indicate stars with and without planets, respectively. This abundance ratio was found to discriminate dwarfs with respect to their planet-harboring status, in a similar role to that played by the linear discriminant indices.

is not very well represented in our analysis, but the result for barium is intriguing and deserves further investigation;

c) vanadium is the element having the most significant abundance difference between giant planet hosts and single dwarfs, and this difference is still significant if only stars with $T_{\text{eff}} \lesssim 6000$ K are used;

d) by combining together the elements from Mg to Cu according to Eq. 1, we found a significant overabundance, for the same metallicity, in giant planet hosts in comparison with our sample of single dwarfs;

e) based on the classification tree analysis we have found that abundances of copper and calcium are special discriminators of dwarfs with and without giant planets (over the $[\text{X}/\text{H}]$ scale);

f) by means of a linear discriminant analysis, we have found that $[\text{V}/\text{Ca}]$ seems to be a good abundance ratio for discriminating dwarfs with giant planets.

Acknowledgements. R. da Silva thanks the Instituto Nacional de Pesquisas Espaciais (INPE) for its financial support in the form of a grant (PCI-DA 300.422/2011-3, MCTI/INPE/CNPq). We thanks Jorge Meléndez for critically reading the manuscript. This research has made use of the SIMBAD database, operated at CDS, Strasbourg, France.

References

- Adibekyan, V.Zh., Santos, N.C., Sousa, S.G., et al. 2012a, *A&A*, 543, A89
 Adibekyan, V.Zh., Sousa, S.G., Santos, N.C., et al. 2012b, *A&A*, 545, A32
 Adibekyan, V.Zh., González Hernández, J.I., Delgado Mena, E., et al. 2014, *A&A*, 564, L15
 Anders, E., & Grevesse, N. 1989, *Geochim. Cosmochim. Acta*, 53, 197
 Baranne, A., Queloz, D., Mayor, M., et al. 1996, *A&AS*, 119, 373-390
 Bertran de Lis, S., Delgado Mena, E., Adibekyan, V.Zh., Santos, N.C., & Sousa, S.G. 2015, *A&A*, accepted
 Bond, J.C., Tinney, C.G., Butler, R.P., et al. 2006, *MNRAS*, 370, 163
 Breiman, L., Friedman, J.H., Olshen, R.A., & Stone, C.J. 1984. In *Classification and regression trees*. Chapman and Hall/CRC.
 Bubar, E.J., King, J.R. 2010, *AJ*, 140, 293
 Brugamyer, E., Dodson-Robinson, S.E., Cochran, W.D., & Sneden, C. 2011, *ApJ*, 738, 97
 Chromey, F.R., Faber, S.M., Wood, A., & Danziger, I.J. 1969, *ApJ*, 158, 599

- da Silva, R., Milone, A., & Reddy, B.E. 2011, *A&A*, 526, A71
- Dehnen, W., & Binney, J.J. 1998, *MNRAS*, 298, 387
- Delgado Mena, E.D., Israelian, G., González Hernández, J.I. et al. 2010, *ApJ*, 725, 2349
- Díaz-Cordovés, J., Claret, A., & Giménez, A. 1995, *A&AS*, 110, 329
- Ecuivillon, A., Israelian, G., Santos, N.C., et al. 2004, *A&A*, 418, 703
- Ecuivillon, A., Israelian, G., Santos, N.C., et al. 2006, *A&A*, 445, 633
- Eggen, O.J. 1950, *ApJ*, 111, 65
- ESA 1997, *The Hipparcos and Tycho Catalogues*, ESA SP-1200
- Fischer, D.A., & Valenti, J. 2005, *ApJ*, 622, 1102
- Flower, P.J. 1996, *ApJ*, 469, 355
- Gilli, G., Israelian, G., Ecuivillon, A., Santos, N.C., & Mayor, M. 2006, *A&A*, 449, 723
- Gonzalez, G., Laws, C., Tyagi, S., & Reddy, B.E. 2001, *AJ*, 121, 432
- Gonzalez, G. 2006, *PASP*, 118, 1494
- Gonzalez, G., & Laws, C. 2007, *MNRAS*, 378, 1141
- González Hernández, J.I., Israelian, G., Santos, N.C., et al. 2010, *ApJ*, 720, 1592
- González Hernández, J.I., Delgado Mena, E., Sousa, S.G., et al. 2013a, *Astron. Nachr.*, 334, 172
- González Hernández, J.I., Delgado Mena, E., Sousa, S.G., et al. 2013b, *A&A*, 552, A6
- Guenther, D.B., & Demarque, P. 1997, *ApJ*, 484, 937
- Holmberg, J., Nordström, B., & Andersen, J. 2007, *A&A*, 475, 519
- Iben, I., Jr. 1991, *ApJS*, 76, 55
- Johnson, D.R.H., & Soderblom, D.R. 1987, *AJ*, 93, 864
- Kang, W., Lee, S.-G., & Kim, K.-M. 2011, *ApJ*, 736, 87
- Kim, Y.-C., Demarque, P., Yi, S.K., & Alexander, D.R. 2002, *ApJS*, 143, 499
- Komatsu, E., Smith, K.M., Dunkley, J., et al. 2011, *ApJS*, 192, 18
- Korotin, S., Mishenina, T., Gorbaneva, T., & Soubiran, C. 2011, *MNRAS*, 415, 2093
- Kupka, F., Piskunov, N.E., Ryabchikova, T.A., Stempels, H.C., & Weiss, W.W. 1999, *A&AS*, 138, 119
- Kupka, F., Ryabchikova, T.A., Piskunov, N.E., Stempels, H.C., & Weiss, W.W. 2000, *BaltA*, 9, 590
- Kurucz, R.L., Furenlid, I., Brault, J., & Testerman, L. 1984, in *The Solar Flux Atlas from 296 nm to 1300 nm*, National Solar Observatory
- Kurucz, R. 1993, CD-ROM No. 13, *ATLAS 9 Stellar Atmosphere Programs and 2 km s⁻¹ Grid* (Cambridge, Mass.: Smithsonian Astrophysical Observatory)
- Kurucz, R. 1995, CD-ROM No. 18, *An Atomic and Molecular Data Bank for Stellar Spectroscopy*, ASP Conference No. 81
- Liu, Y., Sato, B., & Zhao, G. 2010, *PASJ*, 62, 1071
- Lodders, K., Palme, H., & Gail, H.-P. 2009, In *Landolt-Börnstein, New Series, Vol. VI/4B, Chap. 4.4*, J.E. Trümper (ed.), Berlin, Heidelberg, New York: Springer-Verlag, p. 560-630
- Mata Sánchez, D., González Hernández, J.I., Israelian, G., et al. 2014, *A&A*, 566, 83
- Meléndez, J., Asplund, M., Gustafsson, B., & Yong, D., *ApJ*, 704, L66
- Montes, D., López-Santiago, J., Gálvez, M.C., et al. 2001, *MNRAS*, 328, 45
- Moore, C.E., Minnaert, M., & Houtgast, J. 1966, in *The Solar Spectrum 2935 Å to 8770 Å*, Nat. Bur. Std., US Monograph 61
- Moultaka, J., Il'ovaisky, S.A., Prugniel, P., & Soubiran, C. 2004, *PASP*, 116, 693
- Neves, V., Santos, N.C., Sousa, S.G., Correia, A.C.M., & Israelian, G. 2009, *A&A*, 497, 563
- Petigura, E.A., & Marcy, G.W. 2011, *ApJ*, 735, 41
- Piskunov, N.E., Kupka, F., Ryabchikova, T.A., Weiss, W.W., & Jeffery, C.S. 1995, *A&AS*, 112, 525
- Ramírez, I., Meléndez, J., & Asplund, M. 2009, *A&A*, 508, L17
- Ramírez, I., Asplund, M., Baumann, P., Meléndez, J., & Bensby, T. 2010, *A&A*, 521, A33
- Reddy, B.E., Lambert, D.L., & Prieto, C.A. 2006, *MNRAS*, 367, 1329
- Robinson, S.E., Laughlin, G., Bodenheimer, P., & Fischer, D. 2006, *ApJ*, 643, 484
- Ryabchikova, T.A., Piskunov, N.E., Kupka, F., & Weiss, W.W. 1997, *BaltA*, 6, 244
- Sandage, A., & Fouts, G. 1986, *AJ*, 91, 1140
- Santos, N.C., Israelian, G., & Mayor, M. 2001, *A&A*, 373, 1019
- Santos, N.C., Israelian, G., & Mayor, M. 2004, *A&A*, 415, 1153
- Smiljanic, R., Porto de Mello, G.F., & da Silva, L. 2007, *A&A*, 468, 679
- Smith, V.V., Cunha, K., & Lazzaro, D. 2001, *AJ*, 121, 3207
- Snedden, C. 2002, <http://verdi.as.utexas.edu/moog.html>
- Sousa, S.G., Santos, N.C., Israelian, G., Mayor, M., & Monteiro, J.P.F.G. 2007, *A&A*, 469, 783
- Steffen, M. 1985, *A&AS*, 59, 403
- Takeda, Y., Sato, B., & Murata, D. 2008, *PASJ*, 60, 781
- Torres, G. 2010, *AJ*, 140, 1158
- van Leeuwen, F. 2007, *Astrophysics and Space Science Library*, Vol. 350, *Hipparcos, the New Reduction of the Raw Data*
- Wallace, L., Hinkle, K.H., Livingston, W.C., & Davis, S.P. 2011, *ApJS*, 195, 6
- Williams, P.M. 1971, *The Observatory*, 91, 37
- Yi, S., Demarque, P., Kim, Y.-C., et al. 2001, *ApJS*, 136, 417
- Zács, L. 1994, *A&A*, 283, 937

Table 2. Atomic line parameters of the elements used in the analysis and *EW*s measured in the degraded spectrum of the Solar Flux Atlas.

λ [Å]	Id.	χ [eV]	$\log gf$	<i>EW</i> [mÅ]	λ [Å]	Id.	χ [eV]	$\log gf$	<i>EW</i> [mÅ]	λ [Å]	Id.	χ [eV]	$\log gf$	<i>EW</i> [mÅ]
5247.06	Fe I	0.09	-5.022	64.0	6265.14	Fe I	2.18	-2.588	87.4	5426.24	Ti I	0.02	-2.778	11.3
5322.05	Fe I	2.28	-2.878	62.6	6380.75	Fe I	4.19	-1.315	53.6	5471.20	Ti I	1.44	-1.558	7.7
5501.48	Fe I	0.96	-3.105	121.2	6498.94	Fe I	0.96	-4.608	47.4	5490.15	Ti I	1.46	-0.994	22.1
5522.45	Fe I	4.21	-1.397	46.1	6608.03	Fe I	2.28	-3.945	18.1	5648.57	Ti I	2.49	-0.378	10.8
5543.94	Fe I	4.22	-1.055	64.7	6627.55	Fe I	4.55	-1.476	28.5	5679.94	Ti I	2.47	-0.690	5.9
5546.51	Fe I	4.37	-1.098	54.6	6703.57	Fe I	2.76	-3.010	37.8	5739.46	Ti I	2.25	-0.802	7.3
5560.22	Fe I	4.43	-1.080	52.8	6726.67	Fe I	4.61	-1.060	47.4	5866.45	Ti I	1.07	-0.812	50.2
5587.58	Fe I	4.14	-1.738	32.0	6733.16	Fe I	4.64	-1.434	26.9	6064.63	Ti I	1.05	-1.888	9.3
5618.64	Fe I	4.21	-1.310	50.9	6750.16	Fe I	2.42	-2.638	74.7	6091.18	Ti I	2.27	-0.422	15.8
5619.60	Fe I	4.39	-1.422	36.2	6752.71	Fe I	4.64	-1.206	37.8	6126.22	Ti I	1.07	-1.352	24.7
5633.95	Fe I	4.99	-0.379	69.0	5234.63	Fe II	3.22	-2.196	88.1	6258.10	Ti I	1.44	-0.440	52.0
5635.83	Fe I	4.26	-1.598	33.6	5325.56	Fe II	3.22	-3.237	40.3	4568.35	Ti II	1.22	-2.796	31.4
5638.27	Fe I	4.22	-0.828	79.2	5414.07	Fe II	3.22	-3.574	26.8	4583.42	Ti II	1.16	-2.934	28.1
5641.44	Fe I	4.26	-0.997	66.6	5425.25	Fe II	3.20	-3.235	41.5	4657.21	Ti II	1.24	-2.312	52.9
5649.99	Fe I	5.10	-0.818	35.0	5991.38	Fe II	3.15	-3.568	30.2	4798.54	Ti II	1.08	-2.664	44.4
5651.47	Fe I	4.47	-1.733	19.6	6084.11	Fe II	3.20	-3.770	21.1	5211.54	Ti II	2.59	-1.484	33.3
5652.32	Fe I	4.26	-1.700	28.8	6149.25	Fe II	3.89	-2.719	36.5	5336.78	Ti II	1.58	-1.638	72.0
5653.87	Fe I	4.39	-1.388	38.0	6247.56	Fe II	3.89	-2.290	55.4	5381.02	Ti II	1.57	-1.866	61.8
5661.35	Fe I	4.28	-1.813	23.3	6369.46	Fe II	2.89	-4.150	18.6	5418.76	Ti II	1.58	-2.106	50.0
5662.52	Fe I	4.18	-0.628	95.5	6416.93	Fe II	3.89	-2.618	41.1	5657.44	V I	1.06	-	5.8
5667.52	Fe I	4.18	-1.299	53.3	6432.69	Fe II	2.89	-3.545	42.6	5668.36	V I	1.08	-	5.3
5679.03	Fe I	4.65	-0.774	60.3	6456.39	Fe II	3.90	-2.133	62.9	5670.85	V I	1.08	-	19.0
5701.55	Fe I	2.56	-2.218	84.5	6154.23	Na I	2.10	-1.619	38.0	5727.66	V I	1.05	-	8.0
5731.77	Fe I	4.26	-1.150	57.6	6160.75	Na I	2.10	-1.419	52.5	6090.22	V I	1.08	-	35.2
5741.85	Fe I	4.26	-1.624	32.5	4571.10	Mg I	0.00	-	111.6	6135.37	V I	1.05	-	11.5
5752.04	Fe I	4.55	-0.890	58.3	4730.04	Mg I	4.34	-	67.0	6150.15	V I	0.30	-	11.5
5775.08	Fe I	4.22	-1.139	60.4	5711.10	Mg I	4.34	-	109.0	6199.19	V I	0.29	-	13.6
5793.92	Fe I	4.22	-1.620	34.7	5785.29	Mg I	5.11	-1.890	51.0	6216.36	V I	0.28	-	36.4
5806.73	Fe I	4.61	-0.895	54.8	5684.48	Si I	4.95	-1.638	62.8	6274.66	V I	0.27	-	9.8
5809.22	Fe I	3.88	-1.617	51.2	5690.43	Si I	4.93	-1.800	52.9	6285.17	V I	0.28	-	9.4
5814.81	Fe I	4.28	-1.835	22.6	5701.11	Si I	4.93	-1.994	40.4	4626.54	Mn I	4.71	-	29.5
5852.22	Fe I	4.55	-1.183	41.5	5793.08	Si I	4.93	-1.918	45.2	4739.11	Mn I	2.94	-	65.0
5855.08	Fe I	4.61	-1.519	23.0	6145.02	Si I	5.61	-1.420	40.2	5004.89	Mn I	2.92	-	12.2
5856.09	Fe I	4.29	-1.558	34.5	5581.98	Ca I	2.52	-0.780	97.0	5394.67	Mn I	0.00	-	78.6
5862.36	Fe I	4.55	-0.423	89.6	5590.13	Ca I	2.52	-0.829	93.5	5399.48	Mn I	3.85	-	39.2
5905.68	Fe I	4.65	-0.787	59.4	5867.57	Ca I	2.93	-1.566	26.6	5413.68	Mn I	3.86	-	23.5
5916.26	Fe I	2.45	-2.922	55.0	6161.29	Ca I	2.52	-1.362	59.6	5420.35	Mn I	2.14	-	83.6
5927.79	Fe I	4.65	-1.068	43.2	6163.75	Ca I	2.52	-1.295	63.8	5432.55	Mn I	0.00	-	51.6
5929.68	Fe I	4.55	-1.207	40.5	6166.44	Ca I	2.52	-1.188	70.6	5537.77	Mn I	2.19	-	36.4
5930.19	Fe I	4.65	-0.336	90.8	6169.04	Ca I	2.52	-0.842	94.6	6013.50	Mn I	3.07	-	87.0
5934.66	Fe I	3.93	-1.139	76.3	6169.56	Ca I	2.52	-0.621	112.3	6021.80	Mn I	3.07	-	91.2
5983.69	Fe I	4.55	-0.839	61.6	6455.60	Ca I	2.52	-1.415	57.3	5032.72	Ni I	3.90	-1.178	24.9
5984.82	Fe I	4.73	-0.346	85.1	6499.65	Ca I	2.52	-0.954	87.5	5094.41	Ni I	3.83	-1.052	33.3
6024.06	Fe I	4.55	-0.142	113.8	4518.02	Ti I	0.83	-0.394	74.2	5220.30	Ni I	3.74	-1.246	28.7
6027.06	Fe I	4.08	-1.195	65.1	4548.77	Ti I	0.83	-0.438	72.5	5392.33	Ni I	4.15	-1.328	12.7
6056.01	Fe I	4.73	-0.507	73.5	4617.25	Ti I	1.75	0.288	66.3	5435.87	Ni I	1.99	-2.440	52.3
6065.49	Fe I	2.61	-1.687	119.6	4758.12	Ti I	2.25	0.312	44.5	5452.86	Ni I	3.84	-1.482	16.6
6079.01	Fe I	4.65	-1.015	46.4	4759.27	Ti I	2.25	0.340	46.0	5494.88	Ni I	4.10	-1.055	23.0
6082.72	Fe I	2.22	-3.572	34.7	4778.26	Ti I	2.24	-0.380	15.6	5587.85	Ni I	1.93	-2.438	55.8
6094.38	Fe I	4.65	-1.553	20.6	4926.15	Ti I	0.82	-2.240	6.1	5625.31	Ni I	4.09	-0.714	39.3
6096.67	Fe I	3.98	-1.788	38.1	5022.87	Ti I	0.83	-0.452	75.4	5637.13	Ni I	4.09	-0.846	32.8
6151.62	Fe I	2.18	-3.302	50.1	5071.47	Ti I	1.46	-0.738	31.6	6176.81	Ni I	4.09	-0.270	65.3
6157.73	Fe I	4.08	-1.244	63.2	5113.45	Ti I	1.44	-0.846	27.8	6177.24	Ni I	1.83	-3.497	15.8
6165.36	Fe I	4.14	-1.488	46.1	5145.46	Ti I	1.46	-0.626	37.3	6186.71	Ni I	4.10	-0.886	31.5
6180.21	Fe I	2.73	-2.572	60.1	5147.48	Ti I	0.00	-2.154	33.5	6378.26	Ni I	4.15	-0.812	33.2
6188.00	Fe I	3.94	-1.629	48.5	5152.19	Ti I	0.02	-2.088	35.7	5782.14	Cu I	1.64	-	80.5
6200.32	Fe I	2.61	-2.405	74.7	5192.97	Ti I	0.02	-1.012	87.9	5853.69	Ba II	0.60	-0.888	63.3
6226.74	Fe I	3.88	-2.064	29.7	5211.21	Ti I	0.84	-2.120	7.9	6141.73	Ba II	0.70	0.043	114.3
6229.24	Fe I	2.84	-2.860	39.8	5295.78	Ti I	1.07	-1.670	12.5					
6240.65	Fe I	2.22	-3.298	48.7	5219.70	Ti I	0.02	-2.250	28.6					

Notes. Lines with missing *gf* values represent the elements for which the hyperfine structure was taken into account (Mg, V, Mn, and Cu) and the detailed line splitting is shown in Table 3.

Table 3. The gf values for lines with hyperfine structure computed based on the degraded spectrum of the Solar Flux Atlas.

λ [Å]	$\log gf$	λ [Å]	$\log gf$	λ [Å]	$\log gf$
Mg I : 4571.10		V I : 6274.66		Mn I : 5420.35	
4571.078	-6.554	6274.640	-2.150	5420.277	-2.311
4571.087	-6.594	6274.658	-2.150	5420.301	-2.233
4571.096	-5.694	6274.676	-2.150	5420.334	-3.093
Mg I : 4730.04		V I : 6285.17		5420.376	-1.986
4730.031	-3.254	6285.147	-2.160	5420.429	-1.898
4730.038	-3.294	6285.165	-2.160	Mn I : 5432.55	
4730.046	-2.394	6285.183	-2.160	5432.512	-4.348
Mg I : 5711.10		Mn I : 4626.54		5432.540	-4.434
5711.074	-2.716	4626.464	-0.778	5432.565	-4.544
5711.083	-2.756	4626.504	0.017	5432.584	-4.689
5711.091	-1.856	4626.530	-0.231	5432.598	-4.783
V I : 5657.44		4626.565	0.133	Mn I : 5537.77	
5657.418	-1.569	4626.573	-0.327	5537.691	-2.802
5657.436	-1.569	Mn I : 4739.11		5537.710	-2.689
5657.454	-1.569	4739.099	-1.189	5537.738	-2.653
V I : 5668.36		4739.113	-1.330	5537.764	-2.689
5668.344	-1.590	4739.126	-1.485	5537.802	-2.325
5668.362	-1.590	4739.145	-1.042	Mn I : 6013.50	
5668.380	-1.590	4739.167	-2.392	6013.474	-0.704
V I : 5670.85		Mn I : 5004.89		6013.486	-0.914
5670.833	-0.970	5004.878	-2.249	6013.501	-1.045
5670.851	-0.970	5004.892	-2.390	6013.519	-0.724
5670.869	-0.970	5004.905	-2.545	6013.537	-1.302
V I : 5727.66		5004.924	-2.102	Mn I : 6021.80	
5727.643	-1.434	5004.946	-3.452	6021.764	-1.386
5727.661	-1.434	Mn I : 5394.67		6021.780	-1.237
5727.679	-1.434	5394.617	-4.028	6021.797	-0.406
V I : 6090.22		5394.645	-4.114	6021.806	-0.623
6090.234	-0.629	5394.670	-4.224	6021.814	-0.488
6090.216	-0.629	5394.689	-4.369	Cu I : 5782.14	
6090.198	-0.629	5394.703	-4.463	5782.032	-3.554
V I : 6135.37		Mn I : 5399.48		5782.042	-3.857
6135.352	-1.280	5399.435	-0.904	5782.054	-3.156
6135.370	-1.280	5399.446	-1.094	5782.064	-3.207
6135.388	-1.280	5399.479	-0.995	5782.073	-3.511
V I : 6150.15		5399.502	-0.616	5782.084	-2.810
6150.136	-2.030	5399.536	-1.245	5782.086	-3.156
6150.154	-2.030	Mn I : 5413.68		5782.098	-3.156
6150.172	-2.030	5413.613	-1.826	5782.113	-2.810
V I : 6199.19		5413.653	-1.031	5782.124	-2.810
6199.168	-1.960	5413.679	-1.279	5782.153	-2.709
6199.186	-1.960	5413.714	-0.915	5782.173	-2.363
6199.204	-1.960	5413.722	-1.375		
V I : 6216.36					
6216.340	-1.416				
6216.358	-1.416				
6216.376	-1.416				

Table 4. Excerpt from the list of 140 dwarf stars with the photospheric parameters and [Ti/Fe] abundance ratios.

Star	Spectral type	V_{broad} [km s ⁻¹]	$T_{\text{eff}} \pm \sigma$ [K]	$\log g \pm \sigma$	$\xi \pm \sigma$ [km s ⁻¹]	[Fe/H] $\pm \sigma$	[Ti/Fe] $\pm \sigma$
BD+290503	G5	0.00	5180 \pm 50	4.26 \pm 0.20	0.86 \pm 0.31	0.11 \pm 0.07	-0.07 \pm 0.10
HD 10145	G5 V	0.00	5593 \pm 43	4.25 \pm 0.19	0.78 \pm 0.14	0.01 \pm 0.07	0.03 \pm 0.07
HD 10307	G1.5 V	0.00	5913 \pm 49	4.29 \pm 0.22	1.06 \pm 0.09	0.09 \pm 0.06	-0.02 \pm 0.07
HD 10476	K1 V	0.00	5141 \pm 31	4.29 \pm 0.18	0.40 \pm 0.25	-0.05 \pm 0.05	0.02 \pm 0.08
HD 106116	G4 V	0.00	5620 \pm 36	4.22 \pm 0.17	0.84 \pm 0.11	0.16 \pm 0.05	-0.01 \pm 0.09
HD 106516	F9 V	0.00	6401 \pm 158	4.85 \pm 0.39	1.59 \pm 0.66	-0.47 \pm 0.12	0.29 \pm 0.17
HD 10780	K0 V	0.00	5339 \pm 26	4.40 \pm 0.15	0.71 \pm 0.13	0.00 \pm 0.04	0.02 \pm 0.06
HD 108954	F9 V	0.00	6194 \pm 60	4.60 \pm 0.23	1.15 \pm 0.13	0.08 \pm 0.08	0.03 \pm 0.09
HD 109358	G0 V	0.00	5875 \pm 30	4.42 \pm 0.14	1.21 \pm 0.08	-0.22 \pm 0.04	0.03 \pm 0.06
HD 11007	F8 V	0.00	6032 \pm 44	4.16 \pm 0.26	1.39 \pm 0.09	-0.14 \pm 0.06	0.03 \pm 0.09
...

Notes. The broadening velocity V_{broad} is also shown. The whole tables for this and other elements, also for subgiants and giants, are available in electronic form at the CDS.

Table 7. The same as Table 4 but showing photometric and evolutionary parameters together with the population membership.

Star	$B - V$	M_V	dist. [pc]	BC	$\log L$	mass [M_{\odot}]	age [Gyr]	Population group	Remarks	Ref.
HD 10145	0.691	4.84	37.3	-0.106	0.005 \pm 0.026	0.94 \pm 0.03	10.1 ^{+2.5} _{-1.8}	thin		
HD 10476	0.836	5.82	7.5	-0.239	-0.331 \pm 0.006	0.78 \pm 0.04	17.1 ^{+8.2} _{-7.7}	thin	<i>a</i>	
HD 106116	0.701	4.79	34.9	-0.100	0.025 \pm 0.015	1.00 \pm 0.03	7.1 ^{+2.5} _{-1.4}	thin/thick		
HD 106516	0.470	4.36	22.4	0.011	0.150 \pm 0.016	1.05 \pm 0.05	0.2 ^{+1.3} _{-0.2}	thick		
HD 108954	0.568	4.53	21.8	-0.010	0.092 \pm 0.008	-	-	thin	<i>b</i>	
HD 128311	0.973	6.38	16.6	-0.126	-0.603 \pm 0.015	-	0.50	thin	<i>c, d</i> (U)	1,2
HD 124292	0.733	6.18	22.1	-0.143	-0.516 \pm 0.011	-	-	thin	<i>e</i>	3
HD 206860	0.587	4.74	17.9	-0.020	0.017 \pm 0.008	-	0.10	thin	<i>c, d</i> (P)	1,2
HD 25825	0.593	4.50	45.9	-0.021	0.108 \pm 0.052	-	0.65	thin	<i>d</i> (H)	4
HD 42807	0.663	5.17	18.0	-0.070	-0.140 \pm 0.008	-	2.70	thin	<i>d</i> (W)	5
...

Notes. ^(a) Not considered in the abundance analysis because the age uncertainties are larger than 4 Gyr (see Sect. 4.1); ^(b) Mass and age not derived because the star is located outside the evolutionary tracks and isochrones used; ^(c) Star hosting at least one giant planet; ^(d) Member of a stellar moving group (U: Ursa Major; P: Pleiades; H: Hyades; W: Wolf 630); ^(e) Subdwarf candidate.

References. ⁽¹⁾ <http://exoplanet.eu>; ⁽²⁾ Montes et al. (2001); ⁽³⁾ Sandage & Fouts (1986); ⁽⁴⁾ Eggen (1950); ⁽⁵⁾ Bubar & King (2010)